Research Paper

Generating detailed intercellular communication patterns in psoriasis at the single-cell level using social networking, pattern recognition, and manifold learning methods to optimize treatment strategies

Ying Xiong[1], Sidi Li[2], Yunmeng Bai[3], Ting Chen[1], Wenwen Sun[1], Lijie Chen[1], Jia Yu[1], Liwei Sun[1], Chijun Li[1], Jiajian Wang[4,5,6,7,8,9], Bo Wu[1]

[1]Department of Dermatology, Shenzhen Maternity and Child Healthcare Hospital, Shenzhen 518028, China
[2]Institute of Pathology and Southwest Cancer Center, Southwest Hospital, Army Medical University (Third Military Medical University), Chongqing 400038, China
[3]Department of Nephrology, Shenzhen key Laboratory of Kidney Diseases, Shenzhen People's Hospital, The First Affiliated Hospital, School of Medicine, Southern University of Science and Technology, Shenzhen 518055, Guangdong, China
[4]Department of Pediatrics, The Seventh Affiliated Hospital, Sun Yat-Sen University, Shenzhen 518107, Guangdong, China
[5]Scientific Research Center, The Seventh Affiliated Hospital, Sun Yat-Sen University, Shenzhen 518107, Guangdong, China
[6]Clinical Laboratory Department of The Second Affiliated Hospital, School of Medicine, The Chinese University of Hong Kong, Shenzhen and Longgang District People's Hospital of Shenzhen, Shenzhen 518172, China
[7]Center for Energy Metabolism and Reproduction, Shenzhen Institute of Advanced Technology, Chinese Academy of Sciences, Shenzhen 518055, China
[8]Shenzhen Institute of Advanced Technology, Chinese Academy of Sciences, Shenzhen 518055, China
[9]Shenzhen Key Laboratory of Metabolic Health, Shenzhen 518055, China

Correspondence to: Jiajian Wang, Bo Wu; **email:** jiajianwang2019@gmail.com, https://orcid.org/0000-0003-1766-0681; bowu2004@hotmail.com, https://orcid.org/0000-0003-2646-4439
Keywords: communication patterns, single cell transcriptome, cell type-specific regulons (CTSRs), proteomic sequencing, social networking
Received: August 21, 2023 **Accepted:** December 13, 2023 **Published:** January 29, 2024

ABSTRACT

Psoriasis, a complex and recurrent chronic inflammatory skin disease involving various inflammatory cell types, requires effective cell communication to maintain the homeostatic balance of inflammation. However, patterns of communication at the single-cell level have not been systematically investigated. In this study, we employed social network analysis tools, pattern recognition, and manifold learning to compare molecular communication features between psoriasis cells and normal skin cells. Utilizing a process that facilitates the discovery of cell type-specific regulons, we analyzed internal regulatory networks among different cells in psoriasis. Advanced techniques for the quantitative detection of non-targeted proteins in pathological tissue sections were employed to demonstrate protein expression. Our findings revealed a synergistic interplay among the communication signals of immune cells in psoriasis. B-cells were activated, while Langerhans cells shifted into the primary signaling output mode to fulfill antigen presentation, mediating T-cell immunity. In contrast to normal skin cells, psoriasis cells shut down numerous signaling pathways, influencing the balance of skin cell

renewal and differentiation. Additionally, we identified a significant number of active cell type-specific regulons of resident immune cells around the hair follicle. This study unveiled the molecular communication features of the hair follicle cell-psoriasis axis, showcasing its potential for therapeutic targeting at the single-cell level. By elucidating the pattern of immune cell communication in psoriasis and identifying new molecular features of the hair follicle cell-psoriasis axis, our findings present innovative strategies for drug targeting to enhance psoriasis treatment.

INTRODUCTION

Psoriasis is a prevalent chronic inflammatory skin disease, affecting approximately 0.09% to 5% of the global population, yet its causes remain unclear [1–5]. Effective therapy is currently lacking, and relapses are frequent due to both external and internal factors, including psychological stress, bacterial infections, skin damage, and certain drug administrations (such as interferons, beta-blockers, and lithium) [2, 6–8]. The development of psoriasis is intricately linked to the activation, accumulation, and amplification of adaptive immune T cells, innate immune cells (neutrophils, macrophages, and dendritic cells), and resident skin cells (keratinocytes and endothelial cells).

In the pathogenesis of psoriasis, dying keratinocytes and those under stress release nucleic acids and antimicrobial peptides (AMPs, including LL-37), forming immunostimulatory complexes along with negatively charged RNA and free DNA [9–14]. These complexes activate plasmacytoid DCs (pDCs) and myeloid dendritic cells (DCs) via toll-like receptor 7 (TLR7) [12]. Activated plasma cells subsequently secrete type 1 interferons (IFN-α (Interferon Alpha 1), IFN-β), which, in turn, activate myeloid dendritic cells (mDCs) to produce cytokines such as IL-12 (Interleukin 12) and IL-23 (Interleukin 23) [12, 15, 16]. IL-23 also activates mDCs via toll-like receptor 8 (TLR8) [12]. These activated dendritic cells further stimulate T cell differentiation, and the resulting inflammatory cascades among resident immune cells contribute to the pathological changes observed in psoriasis [15, 16]. While extensive research has enhanced our understanding of the causes, progression, and treatment of psoriasis, there has been limited attention given to elucidating the primary modes of signaling among the various subclasses of psoriasis cells involved. Further studies are warranted to improve our comprehension of the underlying molecular biology and to develop new strategies for enhancing the treatment of psoriasis.

The scRNA-seq technique was employed to investigate molecular changes in major cell populations of psoriasis at the single-cell level and their roles in the inflammatory process [17–19]. However, studies on skin inflammation predominantly focus on identifying cell subpopulations, often neglecting their roles and interrelationships. For instance, Cheng et al. explored the transfer and proliferation of epidermal subpopulations among anatomical sites by comparing gene expression. They identified a subpopulation of "channel" keratinocytes with upregulated gap junction protein family genes and cation-transporting ATPase family genes [17]. Reynolds et al. proposed that interactions between endothelial cells and macrophages in inflammatory skin diseases recruit immune cells and help regulate immunity [18, 20]. While some studies concentrate on specific cell subsets, such as the enhanced circulation of memory CD8+ T cells in the skin of patients with psoriatic arthritis (PsA), considered responsible for dysregulating cutaneous immunity and inflammation development [21], or the significance of Tc17 cells (a subset of CD8+ T cells) and CXCL13 (C-X-C Motif Chemokine Ligand 13) in psoriasis [19], few have investigated the coordination of external communication patterns and internal regulatory networks among different cell subsets of psoriasis. This is especially true at the single-cell transcriptome level, where the focus should be on demonstrating how the genetic differences of various cell subtypes affect both internal and external regulatory relationships.

Cell types in solid tissues are not easily captured by scRNA-seq, and the process of suspension preparation is not conducive to collecting and culturing specific cellular taxa, such as neutrophil transcripts with low expression levels [22–24]. When identifying the role of different cell populations and cell communication in enacting immune responses, challenges arise in performing massively parallel sequencing to capture transcripts [25, 26], and the low expression of key cofactors such as affinity receptors and signaling molecules further complicates establishing cell communication patterns [25–27]. Nevertheless, the coordination of messaging among different immune cell subpopulations and intracellular regulatory networks plays a crucial role in the regulation of inflammation and is essential for dissecting the molecular signature of psoriasis. Improved understanding of intercellular communication patterns may enhance the design of new therapeutics, particularly in cell therapy. To address the coordinating relationship between the intracellular

and extracellular components of psoriasis cells, we applied social network analysis tools, pattern recognition methods, and manifold learning approaches to explore communication patterns between cells [28–31]. Utilizing pharmacogenomic data, we identified cell type-specific regulons (IRIS3) involved in the internal regulatory network among different cells in psoriasis. This discovery provides additional evidence for the interconnectedness of the internal regulatory network and external communication patterns, highlighting prospective targets for therapeutic interventions in the hair follicle-psoriasis axis [32, 33]. Furthermore, we employed the most advanced protein pathological section detection technology to identify proteins within a restricted set of diagnosed tissue sections. Subsequently, we established the correlation between the communication patterns of psoriasis cells and their clinical significance. Additionally, we confirmed the validity of the hair follicle axis hypothesis through the examination of pathological specimens [34–37].

RESULTS

Differences in cell communication between psoriatic and normal skin

To investigate and compare cell-cell communication in psoriasis and healthy skin, we gathered single-cell transcriptomic datasets from 5 patients with psoriasis and 3 normal skin volunteers. Cells were categorized into 15 types (Figure 1) based on literature protein markers: B-cells, T-cells, fibroblasts, hair follicles, keratinocytes, Langerhans cells, lymphatic endothelial cells, mast cells, melanocytes, myeloid cells, plasma cells, and Schwann cells. Cellchat was employed for the analysis of scRNA-seq datasets from psoriatic and normal skin.

Comparing cellular communication intensity between psoriasis and normal skin revealed a significant quantitative difference, with 207 for psoriasis and 745 for normal skin (Figure 1A, 1B). Analysis of the interacting cell types demonstrated a positive correlation between the number and intensity of cell communications, but the primary cell populations involved varied significantly between the two states. Normal skin was characterized by a dominance of VSMC (Vascular smooth muscle cells) and T-cells, while psoriatic skin exhibited dominance by Langerhans cells (Figure 1C, 1D).

Further examination of the input and output patterns of communication indicated that the intensity of output signals was primarily dominated by VSMC and T-cells in normal skin, whereas Langerhans cells were the predominant output signals in psoriasis. Sebocytes and T-cells displayed higher intensity in the input signal pattern of psoriatic skin, while lymphatic cells were dominant in normal skin (Figure 1E, 1F). Additionally, we observed relatively weak input and output signals of plasma cells in both physiological states, even though their signaling pathways were active. Weak signals were also generated in normal skin by B-cells and sebocytes, while in psoriasis, certain cell types, notably plasma and Schwann cells, either produced weak signals or no signals at all. Notably, changes in the communication pattern of immune cells in the pathological state were identified: B-cells were activated, and T-cells shifted from predominantly being output signals to predominantly being input signals (Figure 1E, 1F). These findings underscore significant differences in the number of interactions and cell populations between normal and psoriatic skin.

Information flow in psoriatic and normal skin

Differences in cellular information flow between psoriatic and normal skin were calculated based on the sum of communication probabilities between cell populations (Figure 2A, 2B). Our results revealed significant disparities in information flow between psoriatic and normal skin: normal skin exhibited activity in ten signaling pathways (FN1 (Fibronectin 1), EGF (Epidermal Growth Factor), THBS (Thrombospondin 1 pathway), PERIOSTIN (Periostin), MPZ (Myelin Protein Zero), CDH1 (Cadherin 1-mediated signaling pathway), NOTCH (Notch signaling pathways), CD46 (Trophoblast-Lymphocyte Cross-Reactive Antigen), CDH, PDGF (Platelet-Derived Growth Factor)), while psoriasis skin presented two unique signaling pathways (MIF (Macrophage Migration Inhibitory Factor) and APP (Amyloid-Beta Precursor Protein)). Unexpectedly, we identified several communication pathways in normal skin that were relatively more active than psoriatic pathways, including LAMININ (LAMC1-mediated signaling pathways), CD99 (Cell Surface Antigen 12E7), COLLAGEN (Collagen), and DESMOSOME (Desmosome).

Different cell types in different skin states were found to activate distinct signaling or communication pathways (Figure 2C, 2D and Supplementary Figures 1, 2). In normal skin, the primary signaling pathways for T-cells and VSMC included COLLAGEN, LAMININ, FN1, CD99, THBS, PERIOSTIN, MPZ, and PDGF (Figure 2C). In psoriasis, Langerhans cells were predominantly and strongly involved via COLLAGEN and LAMININ pathways (Figure 2D), while a variety of cell types participated in the APP pathway, primarily featuring T-cells in the MIF pathway.

Identification of critical proteins involved in signaling pathways by proteomic sequencing of pathological sections

To scrutinize the expression of a diverse array of critical proteins implicated in signaling pathways, we conducted quantitative proteomic analysis on formalin-fixed and paraffin-embedded (FFPE) skin samples obtained from 9 patients with psoriasis and 6 normal patients, employing state-of-the-art FFPE quantitative proteomics technology (Figure 3A). All specimens, both from psoriatic and normal skin, underwent characterization by two protein groupings through principal component analysis (PCA) (Supplementary Table 1 and Figure 3B, 3C). Pearson's r values consistently exceeded 0.70 across all specimens, with a correlation of 0.92 observed

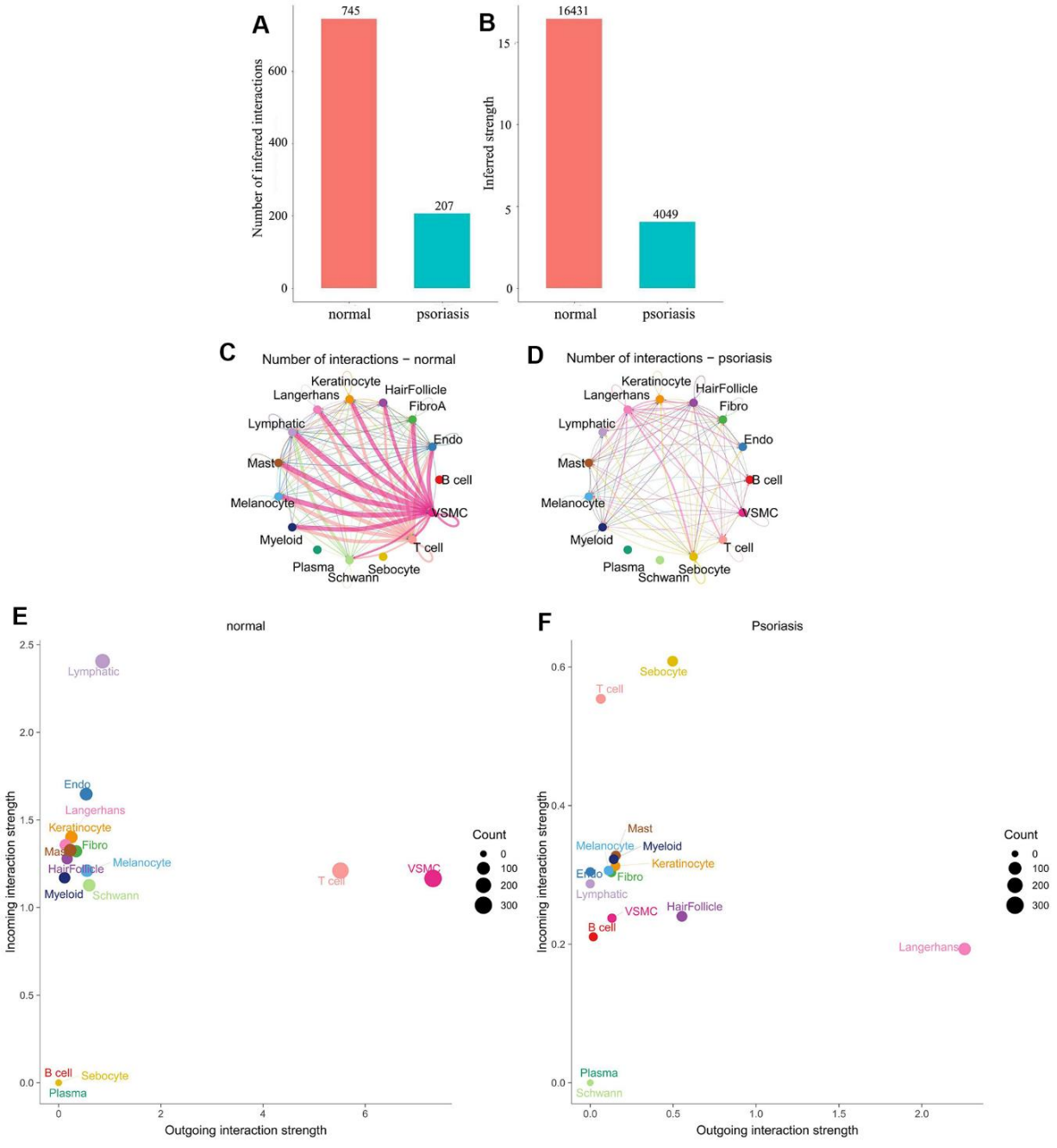

Figure 1. Differences in cell subpopulation communication between psoriatic and normal skin. (**A**, **B**) Differences in the number and intensity of communications. (**C**, **D**) Interaction relationships for each cell subtype. (**E**, **F**) Differences in signal input and signal output patterns.

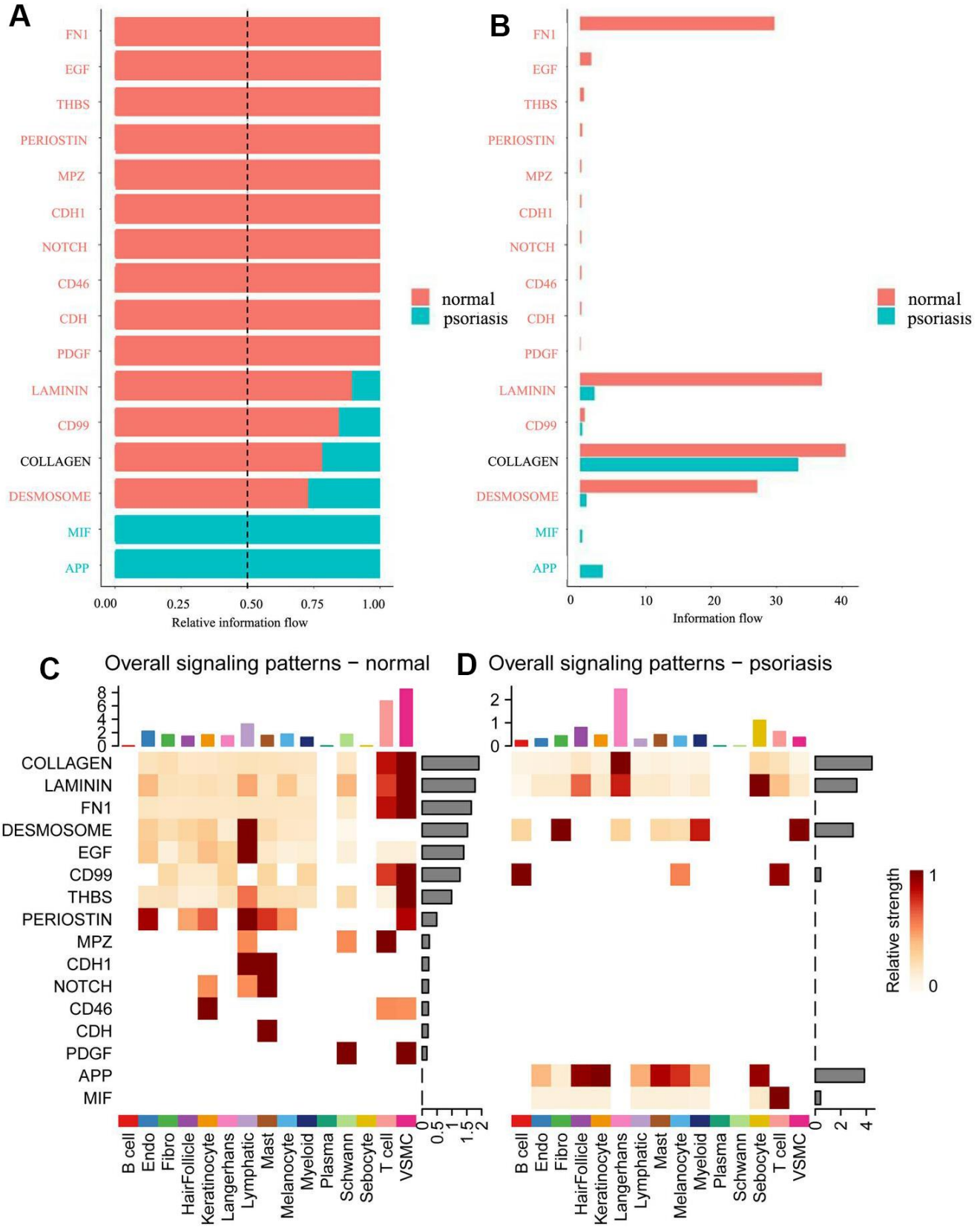

Figure 2. Comparison of information flow between psoriatic and normal skin. (**A**) Relative information flow. (**B**) Information flow. Red represents normal skin, blue represents psoriasis. (**C**) Global signal distribution of each subtype of cells in normal skin. (**D**) Global signal distribution of each subtype of cells in psoriatic skin.

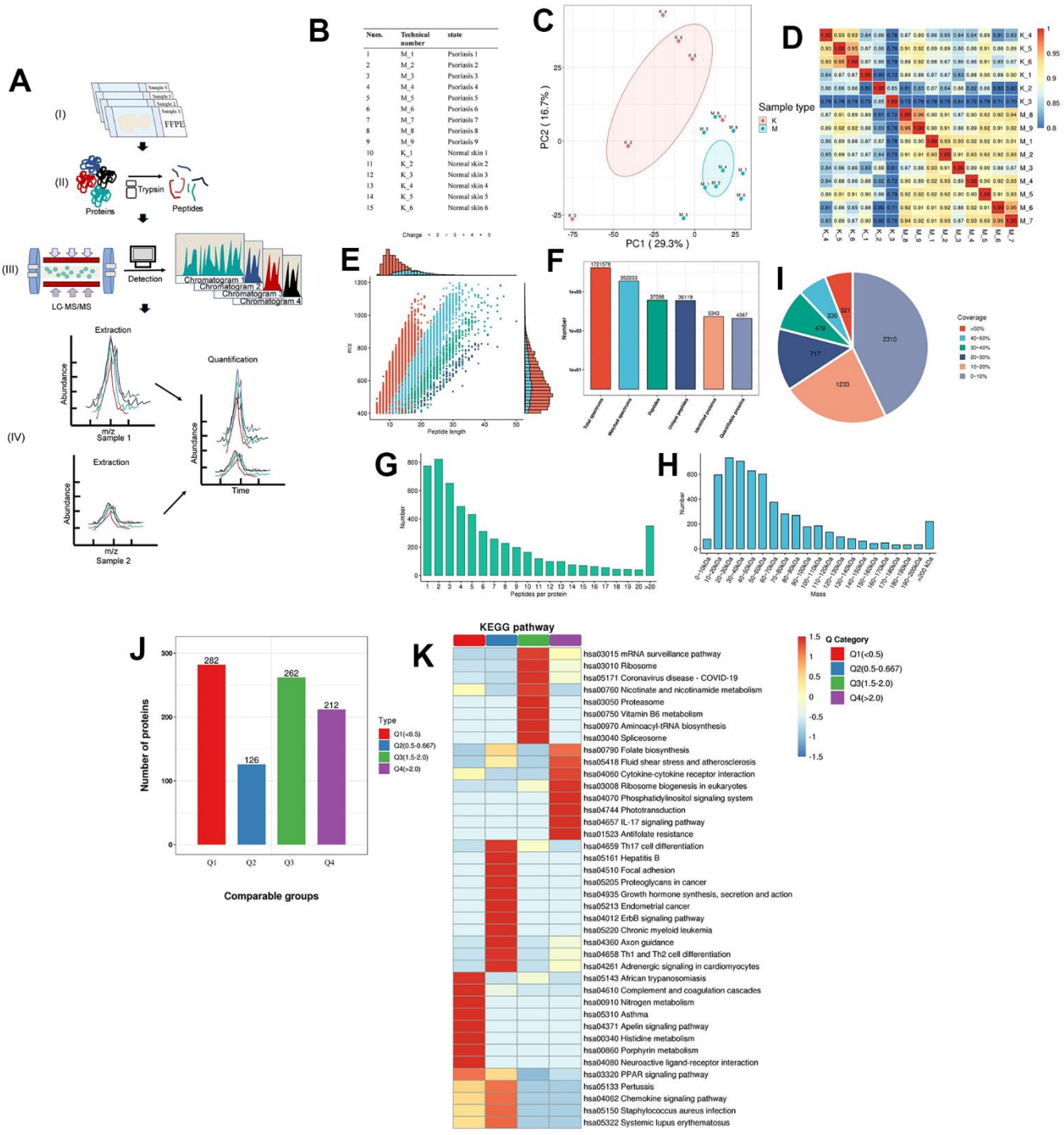

Figure 3. Proteomics of pathological tissue sections in psoriatic skin and normal skin. (**A**) Schematic diagram of the quantitative proteomics sequencing process for formalin-fixed and paraffin-embedded (FFPE) pathology sections. (I) Formalin-fixed and paraffin-embedded (FFPE) pathology section. (II) Enzymatic digestion and extraction of proteins. (III) Schematic diagram of LC-MS/MS. (IV) Label-free quantification. (**B**) Clinical information on patients: 9 patients with psoriasis and 6 specimens of normal skin. (**C**) Principal component cluster analysis for protein quantification of all clinical samples, with the degree of aggregation representing the magnitude of inter-sample variability. The results show that the normal and psoriatic samples clustered to form two major groups, indicating the heterogeneity that exists between the samples and a true reflection of the differences between the two groups. (**D**) Correlation analysis between all samples. The colours and numbers represent the strength of the correlation. (**E**) Peptide length distribution in pathological histological sections of psoriatic skin and normal skin. The vertical axis represents the ratio of charged particle mass to charge, i.e. the mass-to-charge ratio (m/z), and the horizontal axis represents the peptide length, with each point indicating a different peptide segment and the colour indicating a different charge gradient. The bar graph represents the charge. (**F**) Protein identification analysis. Total spectrums: the number of secondary

spectra generated by mass spectrometry. Matched spectrums: the number of valid spectra, the number of spectra matching the theoretical secondary spectrum. Peptides: the number of identified peptides, the number of peptide sequences resolved by matching. Unique peptides: the number of identified unique peptides, the number of unique peptide sequences resolved by matching. Identified proteins: number of identified proteins, number of proteins resolved by specific peptides. Quantifiable proteins: number of proteins quantified by specific peptides. (**G**) Distribution of the number of peptides. (**H**) Protein molecular weight distribution. (**I**) Protein coverage distribution. Most proteins have less than 30% coverage. In a shotgun (bottom-up) technique based on mass spectrometry, the mass spectra scan for peptides with a greater abundance preference. Thus, protein coverage and abundance in the sample are positively correlated. (**J**) Quality classification of differential proteins and their KEGG analysis. The quality of differentially expressed proteins is divided into four levels (see Supplementary Table 7 for details). Light purple indicates Q1, light green indicates Q2, pink indicates Q3, light blue indicates Q4. (**K**) The KEGG pathway of the differential proteins after classification into different groups. Dark red indicates the level of pathway activity. The classical IL-17 pathway is observed in the higher quality Q4 group, which also contains cytokine receptor interactions, further supporting the molecular hypothesis of the follicular psoriasis axis.

between independently prepared tissues from the same psoriasis patient (Figure 3D). The majority of peptides in the specimens comprised 7-20 amino acids, aligning with the general pattern obtained through enzymatic digestion and mass spectrometry fragmentation. The distribution of peptide lengths identified by mass spectrometry adhered to quality control requirements (Figure 3E). Employing a recently described, highly sensitive label-free proteomic workflow capable of accurately quantifying most cellular proteomes, we identified and quantified over 5000 proteins (Figure 3F and Supplementary Table 5) [35, 37]. Permutation-based false discovery rate (FDR) analysis was executed to correct for multiple hypothesis testing in the Proteome Discoverer (v2.4.1.15) environment [38]. Additionally, we observed that the molecular weights of the identified proteins varied at different stages and were evenly distributed (Figure 3G). Most proteins corresponded to more than two peptides, with 10 or fewer defining the majority (Figure 3H). Our monitoring further revealed that the majority of proteins had less than 30% coverage (Figure 3I). In shotgun (also known as bottom-up) based mass spectrometry methods, spectra are preferentially scanned for peptides of higher abundance, suggesting a positive correlation between protein coverage and abundance in the samples.

We observed the detectability of most proteins involved in the aforementioned information pathways in psoriatic skin (Supplementary Table 6 and Supplementary Figures 3, 4), affirming the clinical significance of our results. Additionally, the molecular communication status of psoriatic skin was found to be similar between Caucasian and Chinese groups, providing an advantage for targeted drug development and patient treatment. Moreover, through a comprehensive comparison of globally differentially expressed proteins, categorized into four classes based on the fold of differential expression, we identified interactions among cytokines and receptors beyond the classical IL-17 pathway in psoriasis (Figure 3J, 3K and Supplementary Tables 7, 8, 11–14). These experimental findings underscore that the utilization of pathological sections yielded results consistent with our overarching analysis.

Examining the results of information flow and signaling patterns (Figure 2), it is evident that numerous signaling pathways in normal skin are deactivated in pathological skin. Notably, signaling pathways such as NOTCH and PERIOSTIN, crucial for the renewal of differentiation homeostasis in skin cells, exhibited reduced expression of NOTCH receptors associated with atopic dermatitis [39]. In our investigation of pathological tissue sections of psoriatic skin, we observed very low expression of NOTCH-related proteins, including JAG1 (Jagged Canonical Notch Ligand 1), JAG2 (Jagged Canonical Notch Ligand 2), and NOTCH2 (Neurogenic locus notch homolog protein 2) (Supplementary Table 5). JAG1 and JAG2 were not detected, while NOTCH2 was present in very low abundance. POSTN, responsible for encoding periosteal proteins and collagen expression in the skin, often interacts with ITGAV (Integrin Subunit Alpha V) and ITGB5 (Integrin Subunit Beta 5) between fibroblasts [40]. In normal skin, we observed a higher signal intensity in multiple cell types within the PERIOSTIN pathway compared to psoriasis. Subsequently, we confirmed the upregulation of PERIOSTIN pathway-related protein POSTN expression in pathological sections (Supplementary Table 5; Psoriasis/Normal skin Ratio in POSTN protein: 0.813 (or Normal/Psoriasis skin Ratio in POSTN protein: 1.230), Psoriasis/Normal skin Ratio in ITGAV protein: 0.938 (or Normal/Psoriasis skin Ratio in ITGAV protein: 1.066), Psoriasis/Normal skin Ratio in ITGB5 protein: 0.614 (or Normal/Psoriasis skin Ratio in ITGB5 protein: 1.629)). The involvement of multiple cell types in psoriasis, particularly in the more frequent APP pathway, was further confirmed at the protein level. We identified APP pathway-related ligand receptor proteins, including APP and CD74 (CD74 Antigen), with upregulated protein expression in pathological tissue sections of psoriatic skin (Supplementary Table 5; Psoriasis/Normal skin Ratio in CD74 protein: 1.202; Psoriasis/Normal skin Ratio in MIF protein: 1.239).

Changes in communication patterns in multiple cell subtypes of psoriasis

The pattern recognition approach developed in this study enables the linkage of cell populations and signaling pathways to discern different groups of cells as signal senders or receivers. We identified four outgoing signaling patterns and four incoming signaling patterns as follows (Figure 4):

(1) Outgoing signaling pattern #1 is the APP pathway, predominantly led by keratinocytes and mast cells. When pattern #1 transitions to the incoming pattern, the APP pathway is reinforced by the MIF pathway. The cell types involved are presumed to shift to endothelial, hair follicle, keratinocyte, and lymphatic.

(2) Outgoing pattern #2 involves B-cells, T-cells, and melanocytes, corresponding to the MIF and CD99 signaling pathways, typical in the immune process. In the incoming patterns, B-cells and T-cells fall under pattern #4, which exclusively involves CD99 signaling. Here, the participating cells of outgoing pattern #2, in turn, engage in incoming pattern #4.

(3) Fibro, Myeloid, and VSMC constitute outgoing pattern #3, encompassing the DESMOSOME signaling pathway. Fibro, Myeloid, and VSMC incorporate Langerhans when transitioning to input signaling pattern #2. Here, the participating cells of outgoing pattern #3, in turn, participate in incoming pattern #2.

(4) Hair follicles, Langerhans, and sebocytes contribute to outgoing pattern #4 involving COLLAGEN and LAMININ. When shifted to the input pattern, these three types of cells are engaged in three different incoming signaling pathways: the hair follicle participates in incoming pattern #1, Langerhans in incoming pattern #2, and sebocytes in incoming pattern #3. Here, the participating cells of outgoing pattern #4, known for their flexibility, are again involved in incoming pattern #1, pattern #2, and pattern #3.

These results illustrate that the signaling pathways of different cell types in psoriasis form diverse yet relatively stable communication patterns, identifiable as incoming and outgoing processes. One cell type may synergize with one or more other cell types in one or more pathways to fulfill its role in the pathogenesis of psoriasis. Additionally, we observed that certain cell types, such as plasma cells and Schwann cells, are not implicated in intercellular communication in psoriasis (Figures 1E, 1F, 2C, 2D and Supplementary Figures 1, 2).

The role of hair follicle cells in intercellular communication in psoriasis

Hair follicle cells are widely recognized as the immune sentinels of human skin [6]. Our data corroborate their ability to communicate with a diverse range of cell types (Figure 5) and reveal distinct differences between normal and psoriatic skin in cellular communication pathways and the involvement of ligand-receptor pairs (Supplementary Figures 3, 4 and Supplementary Table 6).

(1) Communication between hair follicle cells and keratinocytes was found to be more robust in psoriasis than in normal skin, with entirely different ligand-receptor pairs: DSG1 (Desmoglein 1) / DSC3 (Desmocollin 3) and HBEGF (Heparin Binding EGF Like Growth Factor) / EGFR (Epidermal Growth Factor Receptor) in normal skin, and APP/CD74, COL4A2 (Collagen Type IV Alpha 2 Chain) / CD44 (Cell Surface Glycoprotein CD44), and LAMC1 (Laminin Subunit Gamma 1) /CD44 in psoriasis.

(2) Communication between hair follicle cells and Langerhan cells was associated with COL4A2/ CD44 and LAMC1/CD44 in psoriasis, contrasting with a relatively weak HBEGF/EGFR ligand-receptor pair in normal skin.

(3) Communication between hair follicles and lymphatic endothelial cells revealed prominent ligand-receptor pairs in normal skin, such as DSG1 and its receptor DSC3, COL6A1 (Collagen Type VI Alpha 1 Chain) and its receptors ITGA2 (Integrin Subunit Alpha 2) and ITGB1 (Integrin Subunit Beta 1), while in psoriasis, they were APP and its receptor CD74, LAMC1 and its receptor CD44, and COL4A2 and its receptor CD44.

(4) Communication between hair follicles and mast cells, melanocytes, and myeloid cells only occurred in psoriasis, focusing on COL4A2/CD44 and APP/ CD74 ligand-receptor pairs.

These results underscore the central role of hair follicles in psoriasis through their interaction with resident immune cells. Hair follicles exhibited heightened communication with immune cells in the superficial skin layer, including keratinocytes and endothelial cells, in terms of ligand-receptor relationships. Notably, we found that virtually all ligand receptors involved in the

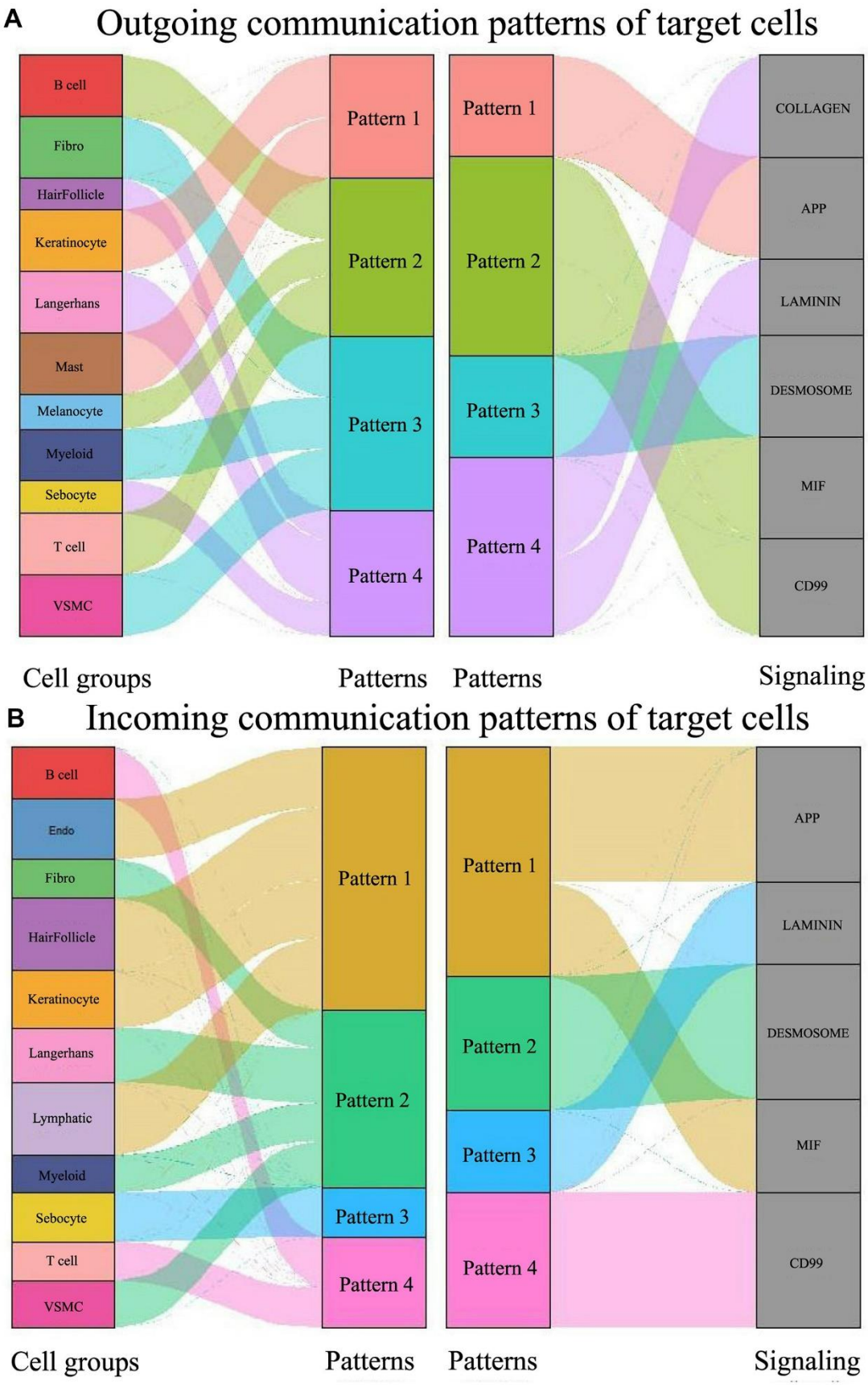

Figure 4. Global signal pattern of each subtype of cells in psoriasis. (**A**) Signal outgoing pattern. (**B**) Signal incoming pattern.

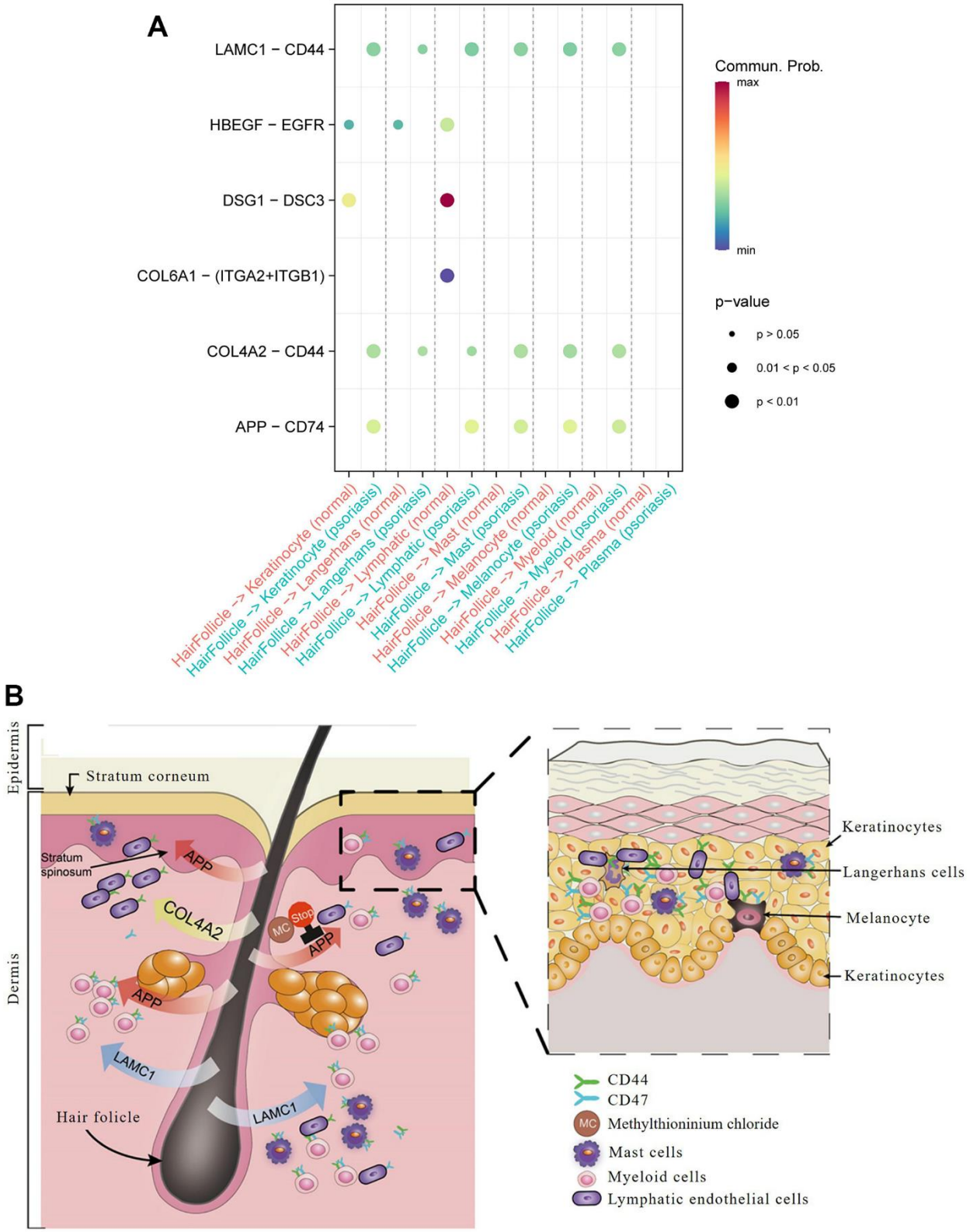

Figure 5. Hair follicle-psoriasis axis at the single cell level. (**A**) Significant ligand-receptor pairs between different subtypes of cells in psoriatic and normal skin. The size of the circles represents significance, and the colour represents the magnitude of the probability of communication between subtypes of cells. (**B**) Diagram of the "hair follicle-psoriasis axis" at the single cell level. Hair follicles release APP, LAMC1 or COL4A2, which communicates with resident immune cells such as melanocytes, mast cells and myeloid cells, thereby activating the immune "garrison" in the local area.

activity of hair follicles and other cell types could be detected in tissue sections of psoriasis patients stored for many years, such as CD74 (Psoriasis/Normal skin Ratio in CD74 protein: 1.202) and CD44 (Psoriasis/Normal skin Ratio in CD44 protein: 1.230) (Supplementary Figures 3, 4 and Supplementary Tables 5, 6). Subcellular localization analysis revealed their predominant concentration extracellularly, further validating their role in inter-cellular interactions (Figure 5 and Supplementary Table 5). This finding holds significance for the collection and preservation of clinical specimens, patient diagnosis, and treatment.

Based on the above analysis, we conclude that LAMC1/CD44, COL4A2/CD44, and APP/CD74 ligand pairs dominate cellular communication in psoriasis. In contrast, the dominant ligand pairs in normal skin are DSG1/DSC3 and HBEGF/EGFR. Therefore, drug targeting of these ligand receptors holds potential clinical benefit in the treatment of psoriasis. The Pharos pharmacogenomic database identified six drugs targeting APP that are already in clinical use: tacrine, methylthioninium chloride, omapatrilat, Florbetapir F-18, Flutemetamol (18F), and florbetaben F18 (Figure 5).

The distribution of cell type-specific regulons (CTSRs) within the intracellular regulatory network and their respective cell subtypes lends support to the hair follicle central axis hypothesis

In addition to exploring external signaling between cells, we delved into the role of the intracellular regulatory network in the central hair follicle-resident immune cell axis by analyzing cell type-specific regulons (CTSRs) (Supplementary Tables 2, 3). Quantitatively, B cells and T cells exhibited zero CTSRs, whereas resident immune cells around the hair follicle, such as keratinocytes, endothelial cells, and fibroblasts, demonstrated active CTSRs. Notably, the abnormal proliferation and differentiation of keratinocytes, a common feature of psoriasis, were validated by the presence of a substantial number of CTSRs (32 CTSRs, Supplementary Tables 2, 3), emphasizing their vital role in maintaining the regulatory network over time [41]. Endothelial cells and fibroblasts, known for their active participation in sustaining the central axis of the hair follicle [42], displayed robust CTSRs. Endothelial cells contributed to early angiogenesis in psoriasis, dependent on mediators like vascular endothelial growth factor, angiopoietin, and pro-angiogenic cytokines (23 CTSRs, Supplementary Tables 2, 3) [42]. Fibroblasts in the skin of psoriasis patients produced a variety of cytokines responsible for the chemical attraction of immune cells proliferating in the dermis and epidermis (16 CTSRs, Supplementary Tables 2, 3) [43].

Particularly noteworthy is the detection of STAT1 (Signal Transducer and Activator of Transcription 1), ZFX (Zinc Finger Protein X-Linked), IRF3 (Interferon Regulatory Factor 3), KLF5 (KLF Transcription Factor 5), NFIB (Nuclear Factor I B), and RXRA (Retinoid X Receptor Alpha) among the regulons during protein analysis of pathological sections. Their presence, upregulated compared to normal skin samples (Supplementary Tables 4, 5) [44], aligns with previous reports. For instance, STAT1, a transcription hub, inhibits the expression of metalloproteinases-3, influencing the cell adhesion molecule pathway and blood vessel formation [44]. STAT1 also affects the activity of the IL-22 promoter, which plays an important role in tissue repair and inflammatory responses [45, 46]. ZFX acts as an important regulator in the proliferation and migration of keratinocytes in skin wound healing. The miR-93-3p/ZFP36L1 (ZFP36 Ring Finger Protein Like 1) /ZFX axis promotes keratinocyte proliferation and migration, thereby affecting skin wound healing [47]. IRF3, a member of the IRF family, is implicated in the STING-IRF3 pathway, suggesting potential improvements in psoriasis treatment through its inhibition [48]. KLF5, a member of the Krupp-like factor subfamily, regulates sphingolipid metabolism and barrier function in the skin [49].

A significant finding supporting the hair follicle-immune cell axis in psoriasis is the involvement of the transcription factor NFIB in the maintenance and regeneration of hair follicles. Knockdown of NFIB and NFIX (Nuclear Factor I X) genes in mice results in the loss of epigenetic characteristics of hair follicle stem cells [50]. Our results indicate the presence of the transcription factor NFIB in keratinocytes, suggesting that the internal regulatory network of keratinocytes influences their interaction with hair follicles during immune regulation [50]. The pathological sectioning assay in our study revealed a substantial overlap exceeding 80% between the identified proteins and the target genes of CTSRs. This not only attests to the robustness of our results but also provides additional evidence of the intricate regulatory network operating within the cell. Specifically, the active factors asso-ciated with CTSRs are predominantly located in hair follicles and neighboring cells, while CTSRs such as B cells and T cells remain inactive (Supplementary Tables 2, 9, 10), aligning with the external communication patterns of the cell. This concurrence underscores the hair follicle central axis hypothesis from both the internal regulatory network and external information exchange patterns.

DISCUSSION

Psoriasis, a multifaceted, chronic inflammatory skin condition involving diverse cell types, prompted our overarching objective: to unravel the communication patterns among these cell subpopulations, particularly focusing on their key ligand-receptor relationships at the single-cell level. This scrutiny aims to enhance therapeutic approaches through targeted interventions. Employing diverse analytical methods such as social network analysis, pattern recognition, and manifold learning techniques [28–31], we visually represented cell communication in this study to substantiate the central axis of hair follicles. Additionally, we leveraged pharmacogenomic information to identify cell type-specific regulons within the internal regulatory network, aligning with the external communication patterns, and identifying potential therapeutic targets [32]. Moreover, we utilized cutting-edge technology to discern proteins in limited diseased tissues, establishing a correlation between cellular communication patterns in psoriasis and their clinical implications. Furthermore, we confirmed the validity of the hair follicle central axis theory using pathological specimens.

Immunosynergistic patterns of multiple immune cells in psoriasis

Previous investigations indicate an elevation of transitional B-cells in the peripheral blood of psoriasis patients compared to normal subjects, potentially as a compensatory mechanism triggered by inflammation [51–53]. Nevertheless, our data unveils a synchronization of immune cell communication in psoriasis, activating B-cells into an input signaling pattern that synergistically reinforces T-cell input signaling. In contrast, T-cells in normal skin exhibit a signaling output pattern, with B-cell signaling in an inactive state, underscoring the pivotal role of B-cells in psoriasis. This marks the inaugural report of a synergistic communication relationship between psoriatic B-cells and T-cells at the single-cell level.

Langerhans cells function as integral components of the dendritic cell immune regulatory network [54–56]. In response to antigenic stimulation, Langerhans cells migrate to locally draining lymph nodes, presenting antigenic peptides to T-cells, thereby initiating an antigen-specific immune response [54–56]. Our results unequivocally demonstrate that Langerhans cells dominate the output signaling pattern in psoriasis, primarily through the COLLAGEN and LAMININ signaling pathways. Beyond immune cell synergy, we identified hair follicle cells as mediators of communication among various cell types in psoriasis through the APP ligand. APP, a hallmark of skin aging, may contribute to the development of psoriatic inflammation [57].

Shutdown of active signaling pathways in psoriasis

The cell communication patterns elucidated in this study reveal substantial suppression of normal T-cell signaling pathways (COLLAGEN, LAMININ, FN1, MPZ, and CD46) in psoriatic skin. Notably, only CD99 signaling remains consistently active, accompanied by MIF signaling. This suggests that CD99 serves as the foundational signal maintaining skin integrity, while MIF signaling emerges as a pivotal immune activation signal. In contrast, B-cells, primarily utilizing CD99, are prevalent in psoriasis, indicating a convergence of signaling pathways between these two immune cell types, potentially facilitating effective transmission and feedback of immune signals.

Of particular interest, psoriasis demonstrates the suppression of THBS, PERIOSTIN, MPZ, CDH1, NOTCH, CD46, CDH, and PDGF signaling pathways. THBS signaling's impact on skin angiogenesis [58, 59], PERIOSTIN's potential role in skin barrier dysfunction [58], and NOTCH signaling's significance in the renewal of differentiated homeostasis in skin cells, with reduced expression linked to atopic dermatitis [39], underscore the intricate regulation occurring in psoriatic skin. Overall, the observed communication patterns among cells lean towards maintaining pathways that promote inflammation, such as APP and MIF, while actively inhibiting those associated with inflammation reduction.

The hair follicle-psoriasis axis and its potential for therapeutic targeting

Abundant evidence substantiates the hair follicle-psoriasis hypothesis. Scalp psoriasis, for instance, correlates with sebaceous gland atrophy [60, 61]. The outer root sheath of the hair follicle houses melanocytes, Langerhans cells, and maintains close associations with resident immune cells such as keratinocytes, lymphatic endothelial cells, and mast cells, crucial for immune recruitment and activation [62–65]. The proximity of Langerhans cells, primary antigen-presenting cells in the epidermis [66], favors the hair follicle's role in activating the local immune 'garrison'. Our single-cell level analysis confirms the intricate communication of hair follicle cells with various cell types. Notably, our data aligns with the "hair follicle immune privilege" hypothesis, revealing no communication between hair follicle cells and effector T-cells [62, 65, 67, 68]. Instead, resident immune cells surrounding the hair follicle appear to play a pivotal role in immune regulation. Moreover,

the communication patterns indicate a shift in the signaling pattern of psoriatic T-cells from an output to an input mode, potentially influenced by signals received from resident immune cells associated with the hair follicle.

Conventional anti-psoriatic drugs (e.g., dithranol, glucocorticoids, and cyclosporine A) necessitate uptake by skin cells to exert pharmacological effects. However, our study suggests an avenue for enhancing psoriasis treatment by inhibiting intercellular signaling pathways conducive to inflammation, such as APP. Six drugs targeting APP, already in clinical use for other diseases, were identified. Notably, Methylthioninium chloride, employed for years in treating dermatological conditions, particularly fungal inflammation [69, 70], emerged as a potential candidate. Our study of cell communication patterns advocates for clinical trials to rigorously assess the efficacy of these drugs for psoriasis treatment.

In conclusion, social network analysis, pattern recognition, and manifold learning techniques provided insights into communication patterns among diverse cell subtypes in psoriasis. Compared to normal skin, numerous signaling pathways are deactivated in psoriatic skin. Our study unveils the molecular characteristics of the hair follicle-psoriasis axis at the single-cell communication level, highlighting the dominance of resident immune cells in immune regulation and supporting the "immune privilege" hypothesis. Future developments in spatial technologies, including spatial proteomics and spatial single-cell transcriptomes in psoriatic inflammation, promise a more comprehensive understanding of spatially distinct inflammatory cell communication patterns [71–75].

MATERIALS AND METHODS

Single-cell communication pattern derivation

CellChat was utilized to read normalized average scRNA-seq expression levels for psoriatic and normal skin, and to merge cell type information to build the CellChat object format [28]. The ideal number of ligand-receptor pairings was calculated with CellChat's more robust statistical approach "trimean" computeAveExpr which examines the expression levels of particular genes in a reciprocal manner: computeAveExpr(cellchat, features = c("APP"), type = "truncatedMean", trim = 0.1). A cellular communication network was developed using the computeCommunProb function. The likelihood of communication at the pathway level was computed using the computeCommunProbPathway function. The GEO (Gene Expression Omnibus database) dataset (GSE150672) was used to obtain raw single cell transcriptome data for psoriasis and normal skin.

Quantifying single-cell communication patterns

Default settings for parameters cellchat-netAnalysis computeCentrality(cellchat, slot.name = "netP") and netAnalysis signalingRole network (cellchat, signaling = pathways.show, width = 8, height = 2.5, font.size = 10) were employed to initially identify dominant senders, receivers, mediators, and influencers involved in inter-cell communication. Coordination among several signaling channels was examined concurrently, for which selectK(cellchat, pattern = "outgoing") and selectK(cellchat, pattern = "incoming") were used to obtain the number of communication patterns. The identifyCommunicationPatterns and netAnalysis river or netAnalysis dot functions were utilized to assign particular routes and illustrate these probable signaling patterns. Signal pathways were grouped together, and clusters were shown using the computeNetSimilarity, netEmbedding, netClustering, and netVisual embedding functions.

Differential examination of the communication patterns of a single cell

The total number and strength of interactions were compared with the compareInteractions function. xpd = TRUE (cellchat, weight.scale = T), mfrow = c (1,2) netVisual diffInteraction netVisual_ diffInteraction (weight.scale = T, "weight" as measure). The netVisual heatmap function displays the number and intensity of cell interactions as a heat map. The netAnalysis signalingRole scatter function was utilized to examine the various functions of cell populations, such as signal transmission and reception. The netVisual bubble function makes it feasible to identify malfunctioning signaling.

Analysis of cell type-specific regulons (CTSRs) in distinct psoriasis cell subtypes

Single-cell gene expression profiles for psoriasis were organized into Seurat objects. To ensure downstream analysis reliability, genes with zero expression values in >99.9% of cells and cells with fewer than 200 genes expressing zero values were excluded. Subsequently, the bicluster tool QUBIC2 was employed for gene module delineation. Biclusters, representing co-expressed genes in specific cell subpopulations, were identified [76]. The similarity between cells in the cell type cluster and those in the bicluster was examined. The hypothesis was that genes constituting the bicluster would exhibit a regulatory signaling response in specific cell types. Hypergeometric enrichment tests were conducted to assess the consistency of cell types in the dataset and the cell composition of the bicluster. A significant

result (adjusted $P < 0.05$) in cellular hypergeometric tests indicated the activation of the bicluster in the respective cell type. Active gene modules with cell type specificity and motifs were identified in the biclusters. Anticipated functions were determined using MEME and DMINDA2.0 [77, 78], and de novo motif development was performed. Upstream promoter sequences within a 2,000 bp region were selected, using the hg38 reference genome. The R package BSgenome.Hsapiens.UCSC.hg38 provided the hg38 human reference genomes. Motif clustering in distinct cell types was analyzed using TOMTOM [79] and the most similar known motifs were annotated from the HOCOMOCO database [80]. To filter out matching motifs, HOCOMOCO targets with a Q-value larger than 0.05 were excluded. The Q-value represented the false discovery rate at which the observed similarity was considered significant. For each theme cluster, the list of non-redundant genes was designated as a regulon. The regulon activity score (RAS) in the cell was generated based on the ranking of expression levels of all involved genes. An empirical P-value, calculated by comparing the RSS (Regulon Specificity Score) of a regulon against a randomly selected set of genes from the same cell type (by bootstrap method), led to the identification of cell-specific regulons with a P-value of 0.05 or less. The single-cell dataset of mouse skin at various developmental phases was derived from GSE129218.

Analysis of medication targeting based on ligand-receptor combinations on a single cell level

Several ligand-receptor combinations were entered into the Pharos database, and the "bulk search" function was used to find potential psoriasis therapies [81]. Choices were divided into four basic categories: "Tclin" (drugs having a known mechanism of action and FDA approval), "Tchem" (drugs with a small molecule ligand linked to the target protein), "Tbio" (known gene ontology or phenotype), and "Tdark" (not yet studied). Due to its immediate therapeutic significance, the "Tclin" class of medicines was chosen for future investigation.

Clinicopathological samples

A total of 225 clinical pathological samples were collected for proteomic sequencing, of which 135 came from 9 patients with psoriasis and 90 from 6 individuals with normal skin. Supplementary Table 1 provides a summary of the clinicopathological characteristics of all patients included in this study. Prior informed consent was obtained, and the Shenzhen Maternity & Child Healthcare Hospital's Ethics Committee authorized this study (SFYLS [2022] 044).

Mass spectrometric (MS) analysis preparation for formalin-fixed, paraffin-embedded (FFPE) tissue

Psoriatic skin sections and paraffin sections from patients undergoing debulking surgery were collected by pathologists at the Shenzhen Maternal and Child Healthcare Hospital. The stored samples at -80° C were retrieved, dewaxed, and diluted fourfold with lysis buffer (1% Sodium dodecyl sulfate (SDC) containing 1% protease inhibitor). Subsequently, they were de-crosslinked overnight at 56° C, lysed through ultra-sonication, and centrifuged at 12,000 g for 10 minutes. Following centrifugation, removal of cell debris was performed, and the supernatant was carefully transferred to new centrifuge tubes. From each sample, 5 μl of supernatant was extracted for silver staining.

DL-Dithiothreitol (DTT) was introduced to adjust the sample concentration to 5 mM. The samples were then heated at 56° C for 30 minutes after adjusting the volume to match that of the lysate, ensuring equal protein quantities for each sample. Iodoacetamide (IAM) was added to adjust the sample concentration to 11 mM before an incubation at room temperature in the dark for 15 minutes. Urea was diluted with triethylammonium bicarbonate buffer (TEAB) to achieve a concentration of less than 2 M. Trypsin was added to the samples at a ratio of 1:50 (m/m) to protein, thoroughly mixed, and subjected to overnight digestion. An additional 4 hours of digestion were carried out by introducing trypsin to the samples at a ratio of 1:100 (m/m) to protein.

Liquid chromatography-mass spectrometric evaluation of FFPE tissue samples

The peptides were solubilized in mobile phase A and separated using an EASY-nLC 1200 ultra-high-performance liquid chromatography system (LC140, Thermo ScientificTM, Waltham, MA, USA). Mobile phase A comprised an aqueous solution containing 0.1% formic acid and 2% acetonitrile, while mobile phase B consisted of an aqueous solution containing 0.1% formic acid and 90% acetonitrile. The gradient parameters were as follows: 0-70 min, 6%-22% B; 70.0-83.0 min, 22%-34% B; 83.0-87.0 min, 34%-80% B; 87.0-90.0 min, 80% B. After separation, the peptides entered a Nanospray Flex (NSI) ion source (Nanospray FlexTM, Thermo ScientificTM, Waltham, MA, USA) and underwent analysis using a high-resolution Orbitrap ExplorisTM 480 mass spectrometer (Thermo ScientificTM, Waltham, MA, USA).

The ion source voltage was set at 2.2 kV, and the FAIMS compensation voltage (CV) varied between -45 V and -65 V. Peptide parent ions and their secondary

fragments were identified and analyzed by mass spectrometry across the scan range 400 - 1200 m/z, with a resolution set at 60,000. The secondary mass spectrometry scan range was 110 m/z, and the secondary scan resolution was 15,000, with TurboTMT turned off. After the initial scan, the 25 peptide ions with the highest signal intensity were selected using a data-dependent acquisition (DDA) approach. Employing a fragmentation energy of 28%, the peptide parent ions were successively fragmented using the higher-energy collisional dissociation (HCD) cell for secondary mass spectrometry. To enhance data presentation in the output spectra, the automatic gain control (AGC) was set to 100%, the signal threshold was 5.0e4 ions/s, the maximum injection time was set to Auto, and the dynamic exclusion time for tandem mass spectrometry scans was 25 seconds to prevent repeated scanning of the parent ions.

Analysis of unprocessed proteomics data

The raw mass spectrometry data were imported into the library search software, and analytical parameters were configured according to the experimental protocol. The secondary mass spectrometry data were scrutinized using Proteome Discoverer (v2.4.1.15) [38]. Search parameters included Homo_sapiens_9606_SP_20220107.fasta (20376 sequences). An inverse library was incorporated to calculate the false discovery rate (FDR) due to random matching, and a common contamination library was added to the database to eliminate contaminating proteins. The digestion method was specified as Trypsin (Full), with the number of missed sites set to 2. The minimum peptide length was established at 6 amino acid residues, and the maximum number of peptide modifications allowed was 3. The mass error tolerance for primary parent ions was set at 10 ppm, and for secondary fragment ions, it was set at 0.02 Da. Carbamidomethyl (C) was designated as a fixed modification, while Oxidation (M), Acetyl (N-terminus), Met-loss (M), and Met-loss+acetyl (M) were considered variable modifications. The FDR for protein, peptide, and peptide-spectrum matches (PSM) identification was maintained at 1%. To ensure high-quality analysis, additional data filtering was applied to the library search results, requiring identified proteins to contain at least one specific (unique) peptide.

Diversification of the protein's functional properties

Gene Ontology (GO) proteome annotations were extracted from the UniProt-GO database (http://www.ebi.ac.uk/GOA/) [82]. Protein IDs were converted to UniProt IDs and mapped to GO IDs, employing InterProScan and protein sequence-matching algorithms to extend GO functional annotations to newly discovered proteins not annotated by the UniProt-GO database [83]. The proteins were categorized into biological processes, cellular components, and molecular activities based on Gene Ontology annotations. Enrichment analysis for differentially expressed proteins against all identified proteins was conducted using a two-tailed Fisher's exact test. A corrected GO with a p-value below 0.05 was deemed significant.

Enriched pathways were identified using the Kyoto Encyclopedia of Genes and Genomes (KEGG) database. The degree to which differentially expressed proteins were enriched for all discovered proteins was assessed through a two-tailed Fisher's exact test [84]. Significant pathways, determined by a corrected p-value of 0.05 or below, were hierarchically organized according to the KEGG website.

Hierarchical clustering based on the functional classification of differentially expressed proteins (e.g., GOs, domains, pathways, and complexes) was performed. Categories with P-values less than 0.05 enriched in at least one cluster were retained. A filtered P-value matrix was generated using the x = -log10 formula (P-value), and a z-transformation was applied to these x-values for each functional category. The resulting Z-values were clustered in Genesis using one-way hierarchical clustering (Euclidean distance, mean linkage clustering). Clustering associations were visualized using the "heatmap.2" function of the "gplots" or "pheatmap" R packages.

Functional analysis of proteins, including classification into families and prediction of structural domains and significant sites, was conducted using the InterPro database (https://www.ebi.ac.uk/interpro). A two-tailed Fisher exact test assessed the enrichment of differentially expressed proteins for all identified proteins [85], with significance accepted at a p-value less than 0.05 after correction. Enrichment of functional structural domains in differentially expressed proteins was explored using the Pfam database [86], with significance determined by Fisher's exact test at a p-value less than 0.05.

The EggNOG database, known for annotating clusters of homologous proteins or COGs (Clusters of Orthologous Groups) [87], provided comprehensive taxonomic information, homologous protein sequences, phylogenetic tree construction, and functional annotation for each homologous gene cluster, surpassing current databases like the NCBI COG database.

Protein subcellular localization

To predict subcellular localization, we employed WolfPsort, a tool for subcellular localization prediction.

WoLF PSORT is an enhanced version of PSORT/PSORT II specifically designed for predicting eukaryotic sequences [88, 89].

Abbreviations

Names of genes/proteins/cells

APP: Amyloid Beta Precursor Protein; CD44: Cell Surface Glycoprotein CD44; CD46: Membrane Cofactor Protein, Trophoblast-Lymphocyte Cross-Reactive Antigen; CD74: CD74 Antigen, Invariant Polypeptide of Major Histocompatibility Complex, Class II Antigen-Associated; CD99: Cell Surface Antigen 12E7; CDH: Cadherin 1-mediated signaling pathway, mainly involved in cell adhesion, which in turn interferes with cell invasion and metastasis; CDH1: Cadherin 1; COL4A2: Collagen Type IV Alpha 2 Chain; COL6A1: Collagen Type VI Alpha 1 Chain; COLLAGEN: Collagen; CXCL13: C-X-C Motif Chemokine Ligand 13; CTSRs: Cell type-specific regulons; DCs: Myeloid dendritic cells; DESMOSOME: Desmosome, regulons of Cellular Signaling and Adhesion; DSC3: Desmocollin 3; DSG1: Desmoglein 1; EGF: Epidermal Growth Factor; EGFR: Epidermal Growth Factor Receptor; FN1: Fibronectin 1; HBEGF: Heparin Binding EGF Like Growth Factor; ITGA2: Integrin Subunit Alpha 2; ITGAV: Integrin Subunit Alpha V; ITGB1: Integrin Subunit Beta 1; ITGB5: Integrin Subunit Beta 5; IFN-α: Interferon Alpha 1; IL-12: Interleukin 12; IL-23: Interleukin 23; IRF: Interferon-regulated transcription factor family; IRF3: Interferon Regulatory Factor 3; JAG1: Jagged Canonical Notch Ligand 1; JAG2: Jagged Canonical Notch Ligand 2; KLF5: KLF Transcription Factor 5; LAMC1: Laminin Subunit Gamma 1; LAMININ: LAMC1-mediated signaling pathways which are implicated in a variety of biological processes including cell adhesion, differentiation, migration, signaling, neuronal growth and metastasis; MIF: Macrophage Migration Inhibitory Factor; MPZ: Myelin Protein Zero; NFIB: Nuclear Factor I B; |NFIX: Nuclear Factor I X; NOTCH: Notch signaling pathways are involved in cell differentiation, apoptosis, proliferation and cell boundary formation, and are important influences on cell morphogenesis; NOTCH2: Neurogenic locus notch homolog protein 2; pDCs: Plasmacytoid dendritic cells; PDGF: Platelet Derived Growth Factor; PERIOSTIN: POSTN, Periostin; RXRA: Retinoid X Receptor Alpha; STAT1: Signal Transducer and Activator of Transcription 1; Tc17: Tc17, the subtype of CD8 T cells; THBS: Thrombospondin 1 pathway, which is involved in platelet cytoplasmic Ca^{2+} elevation and protein metabolism in response; TLR7: Toll-like receptors 7; TLR8: Toll-like receptors 8; VSMC: Vascular smooth muscle cell; ZFP36L1: ZFP36 Ring Finger Protein Like 1; ZFX: Zinc Finger Protein X-Linked.

Analysis techniques and their associated specialized terminology

AGC: Automatic gain control; BSgenome.Hsapiens. UCSC.hg38: Biostrings objects storing whole genome sequences for Homo sapiens (Human) as supplied by UCSC (hg38, based on GRCh38.p13); Cellchat: An R package that can analyse cell-to-cell communication at the single-cell transcriptome level; CellPhoneDB: A software package, currently available in R and Python, that can use spatial information to define possible interacting cell pairs that share/coexist in a micro-environment; COGs: Clusters of Orthologous Groups; CV: Compensation voltage; DDA: Data-dependent acquisition; DTT: DL-Dithiothreitol; DMINDA 2.0: DNA motif recognition and analysis Version 2 is a finding and identification tool for DNA motifs; EASY-nLC 1200: The Thermo Scientific TM EASY-nLCTM 1200 System is a fully integrated system designed for rapid and reliable proteomics detection; eggNOG: A publicly accessible database including orthology linkages, gene evolutionary histories, and functional annotations; FDA: U.S. Food and Drug Administration; FDR: False discovery rates; FFPE: Formalin fixed paraffin-embedded; GEO: Gene Expression Omnibus database; GO: Gene Ontology; HCD: Higher-energy collisional dissociation; HOCOMOCO: HOmo sapiens COmprehensive MOdel Collection presents the Homo sapiens comprehensive model collection featuring meticulously hand-curated transcription factor binding site models; IAM: Iodoacetamide; IRIS3: An integrative cell-type-specific regulon inference server derived from single-cell RNA-Seq; iTALK: An R toolbox for describing and illustrating intercellular communication; KEGG: Kyoto Encyclopedia of Genes and Genomes; KOG: Clusters of Orthologous Groups in Eukaryotes; MEME: A set of programs for discovering motifs in proteins, DNA, and RNA; MS: Mass spectrometry; NicheNet: A method for predicting ligand-target associations by combining expression data from interacting cells with existing knowledge of signaling and gene regulatory networks; PCA: Principal component analysis; PsA: Psoriatic arthritis; PSM: Peptide-spectrum matches; QUBIC2: or QUalitative BIClustering algorithm Version 2, is an algorithm for clustering and identifying functional gene modules based on gene expression; RAS: Regulon activity score; RSS: Regulon specificity score; SDC: Sodium dodecyl sulfate; SingleCellSignalR: SingleCellSignalR is an R package for inferring inter-cell interactions, which performs the basic operations of identifying subgroups of cell taxa and cell types, and clustering the data; TEAB: Triethylammonium bicarbonate buffer; TOMTOM: An algorithm for discovering

motifs and their similarities; it is a part of the MEME software family; WoLF PSORT: Advanced protein subcellular localization prediction tool.

AUTHOR CONTRIBUTIONS

J.J.W. directed the study and drafted the manuscript. T.C., W.W.S., L.J.C., J.Y., L.W.S., and C.J.L. were actively involved in the execution and completion of experiments. Y.M.B. and S.D.L. made substantial contributions to the analysis. Y.X., T.C., W.W.S., L.J.C., J.Y., L.W.S., and C.J.L. participated significantly in the discussions. All authors have thoroughly reviewed and granted approval for the paper.

ACKNOWLEDGMENTS

We express gratitude to Y.X. for guidance regarding the clinical application of our research, B.W. for facilitating the computational analysis venue, and B.W. for providing valuable feedback and reviewing this manuscript. Special thanks to S.D.L. for improving the quality of abstract images. The research made use of the high-performance computing capabilities of the Dell Precision 7920 Tower workstation.

CONFLICTS OF INTEREST

The authors declare that they have no conflicts of interest.

ETHICAL STATEMENT AND CONSENT

The study was conducted with the approval of the Ethics Committee of Shenzhen Maternity and Child Healthcare Hospital (SFYLS [2022] 044). Prior informed consent was obtained from patients included in this study.

FUNDING

The project was supported by research funding from Affiliated Shenzhen Maternity and Child Healthcare Hospital, Southern Medical University.

REFERENCES

1. Michalek IM, Loring B, John SM. A systematic review of worldwide epidemiology of psoriasis. J Eur Acad Dermatol Venereol. 2017; 31:205–12. https://doi.org/10.1111/jdv.13854 PMID:27573025

2. Parisi R, Iskandar IYK, Kontopantelis E, Augustin M, Griffiths CEM, Ashcroft DM, and Global Psoriasis Atlas. National, regional, and worldwide epidemiology of psoriasis: systematic analysis and modelling study. BMJ. 2020; 369:m1590. https://doi.org/10.1136/bmj.m1590 PMID:32467098

3. Parisi R, Symmons DP, Griffiths CEM, Ashcroft DM, and Identification and Management of Psoriasis and Associated ComorbidiTy (IMPACT) project team. Global epidemiology of psoriasis: a systematic review of incidence and prevalence. J Invest Dermatol. 2013; 133:377–85. https://doi.org/10.1038/jid.2012.339 PMID:23014338

4. Burden-Teh E, Thomas KS, Ratib S, Grindlay D, Adaji E, Murphy R. The epidemiology of childhood psoriasis: a scoping review. Br J Dermatol. 2016; 174:1242–57. https://doi.org/10.1111/bjd.14507 PMID:26928555

5. Prignano F, Rogai V, Cavallucci E, Bitossi A, Hammen V, Cantini F. Epidemiology of Psoriasis and Psoriatic Arthritis in Italy-a Systematic Review. Curr Rheumatol Rep. 2018; 20:43. https://doi.org/10.1007/s11926-018-0753-1 PMID:29846817

6. Ayala-Fontánez N, Soler DC, McCormick TS. Current knowledge on psoriasis and autoimmune diseases. Psoriasis (Auckl). 2016; 6:7–32. https://doi.org/10.2147/PTT.S64950 PMID:29387591

7. Mehrmal S, Uppal P, Nedley N, Giesey RL, Delost GR. The global, regional, and national burden of psoriasis in 195 countries and territories, 1990 to 2017: A systematic analysis from the Global Burden of Disease Study 2017. J Am Acad Dermatol. 2021; 84:46–52. https://doi.org/10.1016/j.jaad.2020.04.139 PMID:32376432

8. Griffiths CEM, Armstrong AW, Gudjonsson JE, Barker JN. Psoriasis. Lancet. 2021; 397:1301–15. https://doi.org/10.1016/S0140-6736(20)32549-6 PMID:33812489

9. Frohm M, Agerberth B, Ahangari G, Stâhle-Bäckdahl M, Lidén S, Wigzell H, Gudmundsson GH. The expression of the gene coding for the antibacterial peptide LL-37 is induced in human keratinocytes during inflammatory disorders. J Biol Chem. 1997; 272:15258–63. https://doi.org/10.1074/jbc.272.24.15258 PMID:9182550

10. Morizane S, Yamasaki K, Mühleisen B, Kotol PF, Murakami M, Aoyama Y, Iwatsuki K, Hata T, Gallo RL. Cathelicidin antimicrobial peptide LL-37 in psoriasis enables keratinocyte reactivity against TLR9 ligands. J Invest Dermatol. 2012; 132:135–43. https://doi.org/10.1038/jid.2011.259 PMID:21850017

11. Lande R, Botti E, Jandus C, Dojcinovic D, Fanelli G, Conrad C, Chamilos G, Feldmeyer L, Marinari B, Chon S, Vence L, Riccieri V, Guillaume P, et al. The antimicrobial

peptide LL37 is a T-cell autoantigen in psoriasis. Nat Commun. 2014; 5:5621.
https://doi.org/10.1038/ncomms6621
PMID:25470744

12. Ganguly D, Chamilos G, Lande R, Gregorio J, Meller S, Facchinetti V, Homey B, Barrat FJ, Zal T, Gilliet M. Self-RNA-antimicrobial peptide complexes activate human dendritic cells through TLR7 and TLR8. J Exp Med. 2009; 206:1983–94.
https://doi.org/10.1084/jem.20090480
PMID:19703986

13. Lande R, Gregorio J, Facchinetti V, Chatterjee B, Wang YH, Homey B, Cao W, Wang YH, Su B, Nestle FO, Zal T, Mellman I, Schröder JM, et al. Plasmacytoid dendritic cells sense self-DNA coupled with antimicrobial peptide. Nature. 2007; 449:564–9.
https://doi.org/10.1038/nature06116 PMID:17873860

14. Abraham RM, Zhang Q, Odum N, Wasik MA. The role of cytokine signaling in the pathogenesis of cutaneous T-cell lymphoma. Cancer Biol Ther. 2011; 12:1019–22.
https://doi.org/10.4161/cbt.12.12.18144
PMID:22236880

15. Lowes MA, Suárez-Fariñas M, Krueger JG. Immunology of psoriasis. Annu Rev Immunol. 2014; 32:227–55.
https://doi.org/10.1146/annurev-immunol-032713-120225 PMID:24655295

16. Schön MP. Adaptive and Innate Immunity in Psoriasis and Other Inflammatory Disorders. Front Immunol. 2019; 10:1764.
https://doi.org/10.3389/fimmu.2019.01764
PMID:31402919

17. Cheng JB, Sedgewick AJ, Finnegan AI, Harirchian P, Lee J, Kwon S, Fassett MS, Golovato J, Gray M, Ghadially R, Liao W, Perez White BE, Mauro TM, et al. Transcriptional Programming of Normal and Inflamed Human Epidermis at Single-Cell Resolution. Cell Rep. 2018; 25:871–83.
https://doi.org/10.1016/j.celrep.2018.09.006
PMID:30355494

18. Reynolds G, Vegh P, Fletcher J, Poyner EFM, Stephenson E, Goh I, Botting RA, Huang N, Olabi B, Dubois A, Dixon D, Green K, Maunder D, et al. Developmental cell programs are co-opted in inflammatory skin disease. Science. 2021; 371:eaba6500.
https://doi.org/10.1126/science.aba6500
PMID:33479125

19. Liu J, Chang HW, Huang ZM, Nakamura M, Sekhon S, Ahn R, Munoz-Sandoval P, Bhattarai S, Beck KM, Sanchez IM, Yang E, Pauli M, Arron ST, et al. Single-cell RNA sequencing of psoriatic skin identifies pathogenic Tc17 cell subsets and reveals distinctions between $CD8^+$ T cells in autoimmunity and cancer. J Allergy Clin Immunol. 2021; 147:2370–80.
https://doi.org/10.1016/j.jaci.2020.11.028
PMID:33309739

20. Popescu DM, Botting RA, Stephenson E, Green K, Webb S, Jardine L, Calderbank EF, Polanski K, Goh I, Efremova M, Acres M, Maunder D, Vegh P, et al. Decoding human fetal liver haematopoiesis. Nature. 2019; 574:365–71.
https://doi.org/10.1038/s41586-019-1652-y
PMID:31597962

21. Leijten EF, van Kempen TS, Olde Nordkamp MA, Pouw JN, Kleinrensink NJ, Vincken NL, Mertens J, Balak DMW, Verhagen FH, Hartgring SA, Lubberts E, Tekstra J, Pandit A, et al. Tissue-Resident Memory CD8+ T Cells From Skin Differentiate Psoriatic Arthritis From Psoriasis. Arthritis Rheumatol. 2021; 73:1220–32.
https://doi.org/10.1002/art.41652 PMID:33452865

22. Wang X, Park J, Susztak K, Zhang NR, Li M. Bulk tissue cell type deconvolution with multi-subject single-cell expression reference. Nat Commun. 2019; 10:380.
https://doi.org/10.1038/s41467-018-08023-x
PMID:30670690

23. Xie X, Shi Q, Wu P, Zhang X, Kambara H, Su J, Yu H, Park SY, Guo R, Ren Q, Zhang S, Xu Y, Silberstein LE, et al. Single-cell transcriptome profiling reveals neutrophil heterogeneity in homeostasis and infection. Nat Immunol. 2020; 21:1119–33.
https://doi.org/10.1038/s41590-020-0736-z
PMID:32719519

24. Giordani L, He GJ, Negroni E, Sakai H, Law JYC, Siu MM, Wan R, Corneau A, Tajbakhsh S, Cheung TH, Le Grand F. High-Dimensional Single-Cell Cartography Reveals Novel Skeletal Muscle-Resident Cell Populations. Mol Cell. 2019; 74:609–21.e6.
https://doi.org/10.1016/j.molcel.2019.02.026
PMID:30922843

25. Hughes TK, Wadsworth MH 2nd, Gierahn TM, Do T, Weiss D, Andrade PR, Ma F, de Andrade Silva BJ, Shao S, Tsoi LC, Ordovas-Montanes J, Gudjonsson JE, Modlin RL, et al. Second-Strand Synthesis-Based Massively Parallel scRNA-Seq Reveals Cellular States and Molecular Features of Human Inflammatory Skin Pathologies. Immunity. 2020; 53:878–94.e7.
https://doi.org/10.1016/j.immuni.2020.09.015
PMID:33053333

26. Vieira Braga FA, Kar G, Berg M, Carpaij OA, Polanski K, Simon LM, Brouwer S, Gomes T, Hesse L, Jiang J, Fasouli ES, Efremova M, Vento-Tormo R, et al. A cellular census of human lungs identifies novel cell states in health and in asthma. Nat Med. 2019; 25:1153–63.
https://doi.org/10.1038/s41591-019-0468-5
PMID:31209336

27. Nguyen A, Khoo WH, Moran I, Croucher PI, Phan TG. Single Cell RNA Sequencing of Rare Immune Cell Populations. Front Immunol. 2018; 9:1553. https://doi.org/10.3389/fimmu.2018.01553 PMID:30022984

28. Jin S, Guerrero-Juarez CF, Zhang L, Chang I, Ramos R, Kuan CH, Myung P, Plikus MV, Nie Q. Inference and analysis of cell-cell communication using CellChat. Nat Commun. 2021; 12:1088. https://doi.org/10.1038/s41467-021-21246-9 PMID:33597522

29. Lee DD, Seung HS. Learning the parts of objects by non-negative matrix factorization. Nature. 1999; 401:788–91. https://doi.org/10.1038/44565 PMID:10548103

30. Zhang L, Zhang S. A General Joint Matrix Factorization Framework for Data Integration and Its Systematic Algorithmic Exploration. IEEE Transactions on Fuzzy Systems. 2020; 28:1971–83. https://doi.org/10.1109/tfuzz.2019.2928518

31. Moon KR, Stanley JS, Burkhardt D, van Dijk D, Wolf G, Krishnaswamy S. Manifold learning-based methods for analyzing single-cell RNA-sequencing data. Current Opinion in Systems Biology. 2018; 7:36–46. https://doi.org/10.1016/j.coisb.2017.12.008

32. Ma A, Wang C, Chang Y, Brennan FH, McDermaid A, Liu B, Zhang C, Popovich PG, Ma Q. IRIS3: integrated cell-type-specific regulon inference server from single-cell RNA-Seq. Nucleic Acids Res. 2020; 48:W275–86. https://doi.org/10.1093/nar/gkaa394 PMID:32421805

33. Aibar S, González-Blas CB, Moerman T, Huynh-Thu VA, Imrichova H, Hulselmans G, Rambow F, Marine JC, Geurts P, Aerts J, van den Oord J, Atak ZK, Wouters J, Aerts S. SCENIC: single-cell regulatory network inference and clustering. Nat Methods. 2017; 14:1083–6. https://doi.org/10.1038/nmeth.4463 PMID:28991892

34. Coscia F, Lengyel E, Duraiswamy J, Ashcroft B, Bassani-Sternberg M, Wierer M, Johnson A, Wroblewski K, Montag A, Yamada SD, López-Méndez B, Nilsson J, Mund A, et al. Multi-level Proteomics Identifies CT45 as a Chemosensitivity Mediator and Immunotherapy Target in Ovarian Cancer. Cell. 2018; 175:159–70.e16. https://doi.org/10.1016/j.cell.2018.08.065 PMID:30241606

35. Coscia F, Watters KM, Curtis M, Eckert MA, Chiang CY, Tyanova S, Montag A, Lastra RR, Lengyel E, Mann M. Integrative proteomic profiling of ovarian cancer cell lines reveals precursor cell associated proteins and functional status. Nat Commun. 2016; 7:12645. https://doi.org/10.1038/ncomms12645 PMID:27561551

36. Aebersold R, Mann M. Mass-spectrometric exploration of proteome structure and function. Nature. 2016; 537:347–55. https://doi.org/10.1038/nature19949 PMID:27629641

37. Cox J, Hein MY, Luber CA, Paron I, Nagaraj N, Mann M. Accurate proteome-wide label-free quantification by delayed normalization and maximal peptide ratio extraction, termed MaxLFQ. Mol Cell Proteomics. 2014; 13:2513–26. https://doi.org/10.1074/mcp.M113.031591 PMID:24942700

38. Klykov O, Steigenberger B, Pektaş S, Fasci D, Heck AJR, Scheltema RA. Efficient and robust proteome-wide approaches for cross-linking mass spectrometry. Nat Protoc. 2018; 13:2964–90. https://doi.org/10.1038/s41596-018-0074-x PMID:30446747

39. Siebel C, Lendahl U. Notch Signaling in Development, Tissue Homeostasis, and Disease. Physiol Rev. 2017; 97:1235–94. https://doi.org/10.1152/physrev.00005.2017 PMID:28794168

40. Deng CC, Hu YF, Zhu DH, Cheng Q, Gu JJ, Feng QL, Zhang LX, Xu YP, Wang D, Rong Z, Yang B. Single-cell RNA-seq reveals fibroblast heterogeneity and increased mesenchymal fibroblasts in human fibrotic skin diseases. Nat Commun. 2021; 12:3709. https://doi.org/10.1038/s41467-021-24110-y PMID:34140509

41. Ni X, Lai Y. Keratinocyte: A trigger or an executor of psoriasis? J Leukoc Biol. 2020; 108:485–91. https://doi.org/10.1002/JLB.5MR0120-439R PMID:32170886

42. Alves-Filho JC, Marcel Silva Melo B, Ryffel B. MMP-9 Mediates Cross-Talk between Neutrophils and Endothelial Cells in Psoriasis. J Invest Dermatol. 2021; 141:716–8. https://doi.org/10.1016/j.jid.2020.09.006 PMID:33752809

43. Iwata H, Haga N, Ujiie H. Possible role of epiregulin from dermal fibroblasts in the keratinocyte hyperproliferation of psoriasis. J Dermatol. 2021; 48:1433–8. https://doi.org/10.1111/1346-8138.16003 PMID:34128258

44. Lu X, Du J, Liang J, Zhu X, Yang Y, Xu J. Transcriptional regulatory network for psoriasis. J Dermatol. 2013; 40:48–53. https://doi.org/10.1111/1346-8138.12000 PMID:23078099

45. Bai L, Fang H, Xia S, Zhang R, Li L, Ochando J, Xu J, Ding Y. STAT1 activation represses IL-22 gene expression

and psoriasis pathogenesis. Biochem Biophys Res Commun. 2018; 501:563–9. https://doi.org/10.1016/j.bbrc.2018.05.042 PMID:29750958

46. Grabarek B, Krzaczyński J, Strzałka-Mrozik B, Wcisło-Dziadecka D, Gola J. The influence of ustekinumab on expression of STAT1, STAT3, STAT4, SOCS2, and IL17 in patients with psoriasis and in a control. Dermatol Ther. 2019; 32:e13029. https://doi.org/10.1111/dth.13029 PMID:31330078

47. Feng X, Zhou S, Cai W, Guo J. The miR-93-3p/ZFP36L1/ZFX axis regulates keratinocyte proliferation and migration during skin wound healing. Mol Ther Nucleic Acids. 2020; 23:450–63. https://doi.org/10.1016/j.omtn.2020.11.017 PMID:33473330

48. Xiaohong L, Zhenting Z, Yunjie Y, Wei C, Xiangjin X, Kun X, Xin L, Lu L, Jun L, Pin C. Activation of the STING-IRF3 pathway involved in psoriasis with diabetes mellitus. J Cell Mol Med. 2022; 26:2139–51. https://doi.org/10.1111/jcmm.17236 PMID:35174638

49. Lyu Y, Guan Y, Deliu L, Humphrey E, Frontera JK, Yang YJ, Zamler D, Kim KH, Mohanty V, Jin K, Mohanty V, Liu V, Dou J, et al. KLF5 governs sphingolipid metabolism and barrier function of the skin. Genes Dev. 2022; 36:822–42. https://doi.org/10.1101/gad.349662.122 PMID:36008138

50. Adam RC, Yang H, Ge Y, Infarinato NR, Gur-Cohen S, Miao Y, Wang P, Zhao Y, Lu CP, Kim JE, Ko JY, Paik SS, Gronostajski RM, et al. NFI transcription factors provide chromatin access to maintain stem cell identity while preventing unintended lineage fate choices. Nat Cell Biol. 2020; 22:640–50. https://doi.org/10.1038/s41556-020-0513-0 PMID:32393888

51. Kahlert K, Grän F, Muhammad K, Benoit S, Serfling E, Goebeler M, Kerstan A. Aberrant B-cell Subsets and Immunoglobulin Levels in Patients with Moderate-to-severe Psoriasis. Acta Derm Venereol. 2019; 99:226–7. https://doi.org/10.2340/00015555-3069 PMID:30320869

52. Hayashi M, Yanaba K, Umezawa Y, Yoshihara Y, Kikuchi S, Ishiuji Y, Saeki H, Nakagawa H. Corrigendum to "IL-10-producing regulatory B cells are decreased in patients with psoriasis" [J. Dermatol. Sci. 81 (2016) 93-100]. J Dermatol Sci. 2017; 86:79. https://doi.org/10.1016/j.jdermsci.2017.01.010 PMID:28209293

53. Alrefai H, Muhammad K, Rudolf R, Pham DA, Klein-Hessling S, Patra AK, Avots A, Bukur V, Sahin U, Tenzer S, Goebeler M, Kerstan A, Serfling E. NFATc1 supports imiquimod-induced skin inflammation by suppressing IL-10 synthesis in B cells. Nat Commun. 2016; 7:11724. https://doi.org/10.1038/ncomms11724 PMID:27222343

54. Wang A, Bai Y. Dendritic cells: The driver of psoriasis. J Dermatol. 2020; 47:104–13. https://doi.org/10.1111/1346-8138.15184 PMID:31833093

55. Cabeza-Cabrerizo M, Cardoso A, Minutti CM, Pereira da Costa M, Reis e Sousa C. Dendritic Cells Revisited. Annu Rev Immunol. 2021; 39:131–66. https://doi.org/10.1146/annurev-immunol-061020-053707 PMID:33481643

56. Kroeger J, Hoppe E, Galiger C, Has C, Franzke CW. Amino acid substitution in the C-terminal domain of collagen XVII reduces laminin-332 interaction causing mild skin fragility with atrophic scarring. Matrix Biol. 2019; 80:72–84. https://doi.org/10.1016/j.matbio.2018.10.003 PMID:30316981

57. Li Y, Wang Y, Zhang W, Jiang L, Zhou W, Liu Z, Li S, Lu H. Overexpression of Amyloid Precursor Protein Promotes the Onset of Seborrhoeic Keratosis and is Related to Skin Ageing. Acta Derm Venereol. 2018; 98:594–600. https://doi.org/10.2340/00015555-2911 PMID:29487944

58. Mitamura Y, Nunomura S, Nanri Y, Ogawa M, Yoshihara T, Masuoka M, Tsuji G, Nakahara T, Hashimoto-Hachiya A, Conway SJ, Furue M, Izuhara K. The IL-13/periostin/IL-24 pathway causes epidermal barrier dysfunction in allergic skin inflammation. Allergy. 2018; 73:1881–91. https://doi.org/10.1111/all.13437 PMID:29528494

59. Detmar M. The role of VEGF and thrombospondins in skin angiogenesis. J Dermatol Sci. 2000; 24 Suppl 1:S78–84. https://doi.org/10.1016/s0923-1811(00)00145-6 PMID:11137400

60. Rittié L, Tejasvi T, Harms PW, Xing X, Nair RP, Gudjonsson JE, Swindell WR, Elder JT. Sebaceous Gland Atrophy in Psoriasis: An Explanation for Psoriatic Alopecia? J Invest Dermatol. 2016; 136:1792–800. https://doi.org/10.1016/j.jid.2016.05.113 PMID:27312025

61. Shin MK, Kim KS, Ahn JJ, Kim NI, Park HK, Haw CR. Investigation of the hair of patients with scalp psoriasis using atomic force microscopy. Clin Exp Dermatol. 2012; 37:156–63. https://doi.org/10.1111/j.1365-2230.2011.04212.x PMID:22340692

62. Paus R, Cotsarelis G. The biology of hair follicles. N Engl J Med. 1999; 341:491–7. https://doi.org/10.1056/NEJM199908123410706 PMID:10441606

63. Staricco RG. Amelanotic melanocytes in the outer sheath of the human hair follicle and their role in the repigmentation of regenerated epidermis. Ann N Y Acad Sci. 1963; 100:239–55. https://doi.org/10.1111/j.1749-6632.1963.tb57123.x PMID:13983438

64. Gilliam AC, Kremer IB, Yoshida Y, Stevens SR, Tootell E, Teunissen MB, Hammerberg C, Cooper KD. The human hair follicle: a reservoir of CD40+ B7-deficient Langerhans cells that repopulate epidermis after UVB exposure. J Invest Dermatol. 1998; 110:422–7. https://doi.org/10.1046/j.1523-1747.1998.00162.x PMID:9540986

65. Kabashima K, Honda T, Ginhoux F, Egawa G. The immunological anatomy of the skin. Nat Rev Immunol. 2019; 19:19–30. https://doi.org/10.1038/s41577-018-0084-5 PMID:30429578

66. Kobayashi T, Naik S, Nagao K. Choreographing Immunity in the Skin Epithelial Barrier. Immunity. 2019; 50:552–65. https://doi.org/10.1016/j.immuni.2019.02.023 PMID:30893586

67. Paus R, Link RE. The psoriatic epidermal lesion and anagen hair growth may share the same "switch-on" mechanism. Yale J Biol Med. 1988; 61:467–76. PMID:2462312

68. Takahashi T, Kamimura A. Cyclosporin a promotes hair epithelial cell proliferation and modulates protein kinase C expression and translocation in hair epithelial cells. J Invest Dermatol. 2001; 117:605–11. https://doi.org/10.1046/j.0022-202x.2001.01452.x PMID:11564166

69. Shen JJ, Jemec GBE, Arendrup MC, Saunte DML. Photodynamic therapy treatment of superficial fungal infections: A systematic review. Photodiagnosis Photodyn Ther. 2020; 31:101774. https://doi.org/10.1016/j.pdpdt.2020.101774 PMID:32339671

70. Martins WK, Santos NF, Rocha CDS, Bacellar IOL, Tsubone TM, Viotto AC, Matsukuma AY, Abrantes ABDP, Siani P, Dias LG, Baptista MS. Parallel damage in mitochondria and lysosomes is an efficient way to photoinduce cell death. Autophagy. 2019; 15:259–79. https://doi.org/10.1080/15548627.2018.1515609 PMID:30176156

71. Lundberg E, Borner GHH. Spatial proteomics: a powerful discovery tool for cell biology. Nat Rev Mol Cell Biol. 2019; 20:285–302. https://doi.org/10.1038/s41580-018-0094-y PMID:30659282

72. Mahdessian D, Cesnik AJ, Gnann C, Danielsson F, Stenström L, Arif M, Zhang C, Le T, Johansson F, Schutten R, Bäckström A, Axelsson U, Thul P, et al. Spatiotemporal dissection of the cell cycle with single-cell proteogenomics. Nature. 2021; 590:649–54. https://doi.org/10.1038/s41586-021-03232-9 PMID:33627808

73. Mund A, Coscia F, Kriston A, Hollandi R, Kovács F, Brunner AD, Migh E, Schweizer L, Santos A, Bzorek M, Naimy S, Rahbek-Gjerdrum LM, Dyring-Andersen B, et al. Deep Visual Proteomics defines single-cell identity and heterogeneity. Nat Biotechnol. 2022; 40:1231–40. https://doi.org/10.1038/s41587-022-01302-5 PMID:35590073

74. Moffitt JR, Lundberg E, Heyn H. The emerging landscape of spatial profiling technologies. Nat Rev Genet. 2022; 23:741–59. https://doi.org/10.1038/s41576-022-00515-3 PMID:35859028

75. Li J, Ma J, Zhang Q, Gong H, Gao D, Wang Y, Li B, Li X, Zheng H, Wu Z, Zhu Y, Leng L. Spatially resolved proteomic map shows that extracellular matrix regulates epidermal growth. Nat Commun. 2022; 13:4012. https://doi.org/10.1038/s41467-022-31659-9 PMID:35817779

76. Xie J, Ma A, Zhang Y, Liu B, Cao S, Wang C, Xu J, Zhang C, Ma Q. QUBIC2: a novel and robust biclustering algorithm for analyses and interpretation of large-scale RNA-Seq data. Bioinformatics. 2020; 36:1143–9. https://doi.org/10.1093/bioinformatics/btz692 PMID:31503285

77. Yang J, Chen X, McDermaid A, Ma Q. DMINDA 2.0: integrated and systematic views of regulatory DNA motif identification and analyses. Bioinformatics. 2017; 33:2586–8. https://doi.org/10.1093/bioinformatics/btx223 PMID:28419194

78. Bailey TL, Boden M, Buske FA, Frith M, Grant CE, Clementi L, Ren J, Li WW, Noble WS. MEME SUITE: tools for motif discovery and searching. Nucleic Acids Res. 2009; 37:W202–8. https://doi.org/10.1093/nar/gkp335 PMID:19458158

79. Gupta S, Stamatoyannopoulos JA, Bailey TL, Noble WS. Quantifying similarity between motifs. Genome Biol. 2007; 8:R24.

https://doi.org/10.1186/gb-2007-8-2-r24 PMID:17324271

80. Kulakovskiy IV, Vorontsov IE, Yevshin IS, Sharipov RN, Fedorova AD, Rumynskiy EI, Medvedeva YA, Magana-Mora A, Bajic VB, Papatsenko DA, Kolpakov FA, Makeev VJ. HOCOMOCO: towards a complete collection of transcription factor binding models for human and mouse via large-scale ChIP-Seq analysis. Nucleic Acids Res. 2018; 46:D252–9. https://doi.org/10.1093/nar/gkx1106 PMID:29140464

81. Sheils TK, Mathias SL, Kelleher KJ, Siramshetty VB, Nguyen DT, Bologa CG, Jensen LJ, Vidović D, Koleti A, Schürer SC, Waller A, Yang JJ, Holmes J, et al. TCRD and Pharos 2021: mining the human proteome for disease biology. Nucleic Acids Res. 2021; 49:D1334–46. https://doi.org/10.1093/nar/gkaa993 PMID:33156327

82. UniProt Consortium. UniProt: the universal protein knowledgebase in 2021. Nucleic Acids Res. 2021; 49:D480–9. https://doi.org/10.1093/nar/gkaa1100 PMID:33237286

83. Zdobnov EM, Apweiler R. InterProScan--an integration platform for the signature-recognition methods in InterPro. Bioinformatics. 2001; 17:847–8. https://doi.org/10.1093/bioinformatics/17.9.847 PMID:11590104

84. Kanehisa M, Goto S. KEGG: kyoto encyclopedia of genes and genomes. Nucleic Acids Res. 2000; 28:27–30. https://doi.org/10.1093/nar/28.1.27 PMID:10592173

85. Blum M, Chang HY, Chuguransky S, Grego T, Kandasaamy S, Mitchell A, Nuka G, Paysan-Lafosse T, Qureshi M, Raj S, Richardson L, Salazar GA, Williams L, et al. The InterPro protein families and domains database: 20 years on. Nucleic Acids Res. 2021; 49:D344–54. https://doi.org/10.1093/nar/gkaa977 PMID:33156333

86. Finn RD, Bateman A, Clements J, Coggill P, Eberhardt RY, Eddy SR, Heger A, Hetherington K, Holm L, Mistry J, Sonnhammer EL, Tate J, Punta M. Pfam: the protein families database. Nucleic Acids Res. 2014; 42:D222–30. https://doi.org/10.1093/nar/gkt1223 PMID:24288371

87. Huerta-Cepas J, Szklarczyk D, Heller D, Hernández-Plaza A, Forslund SK, Cook H, Mende DR, Letunic I, Rattei T, Jensen LJ, von Mering C, Bork P. eggNOG 5.0: a hierarchical, functionally and phylogenetically annotated orthology resource based on 5090 organisms and 2502 viruses. Nucleic Acids Res. 2019; 47:D309–14. https://doi.org/10.1093/nar/gky1085 PMID:30418610

88. Horton P, Park KJ, Obayashi T, Fujita N, Harada H, Adams-Collier CJ, Nakai K. WoLF PSORT: protein localization predictor. Nucleic Acids Res. 2007; 35:W585–7. https://doi.org/10.1093/nar/gkm259 PMID:17517783

89. Stadler C, Rexhepaj E, Singan VR, Murphy RF, Pepperkok R, Uhlén M, Simpson JC, Lundberg E. Immunofluorescence and fluorescent-protein tagging show high correlation for protein localization in mammalian cells. Nat Methods. 2013; 10:315–23. https://doi.org/10.1038/nmeth.2377 PMID:23435261

SUPPLEMENTARY MATERIALS

Supplementary Figures

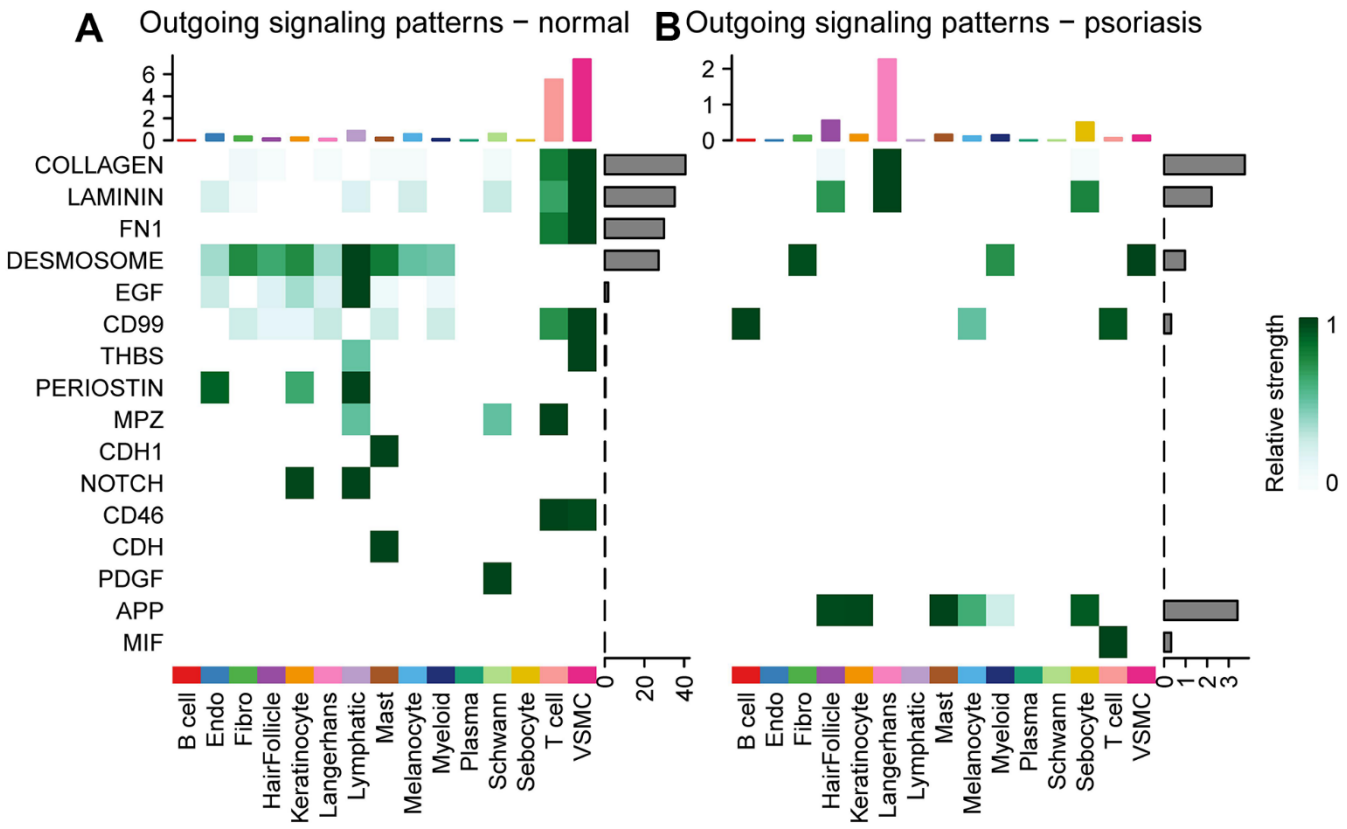

Supplementary Figure 1. Outgoing signaling patterns for each subtype of cells in psoriatic and normal skin. (**A**) Normal skin. (**B**) Psoriasis.

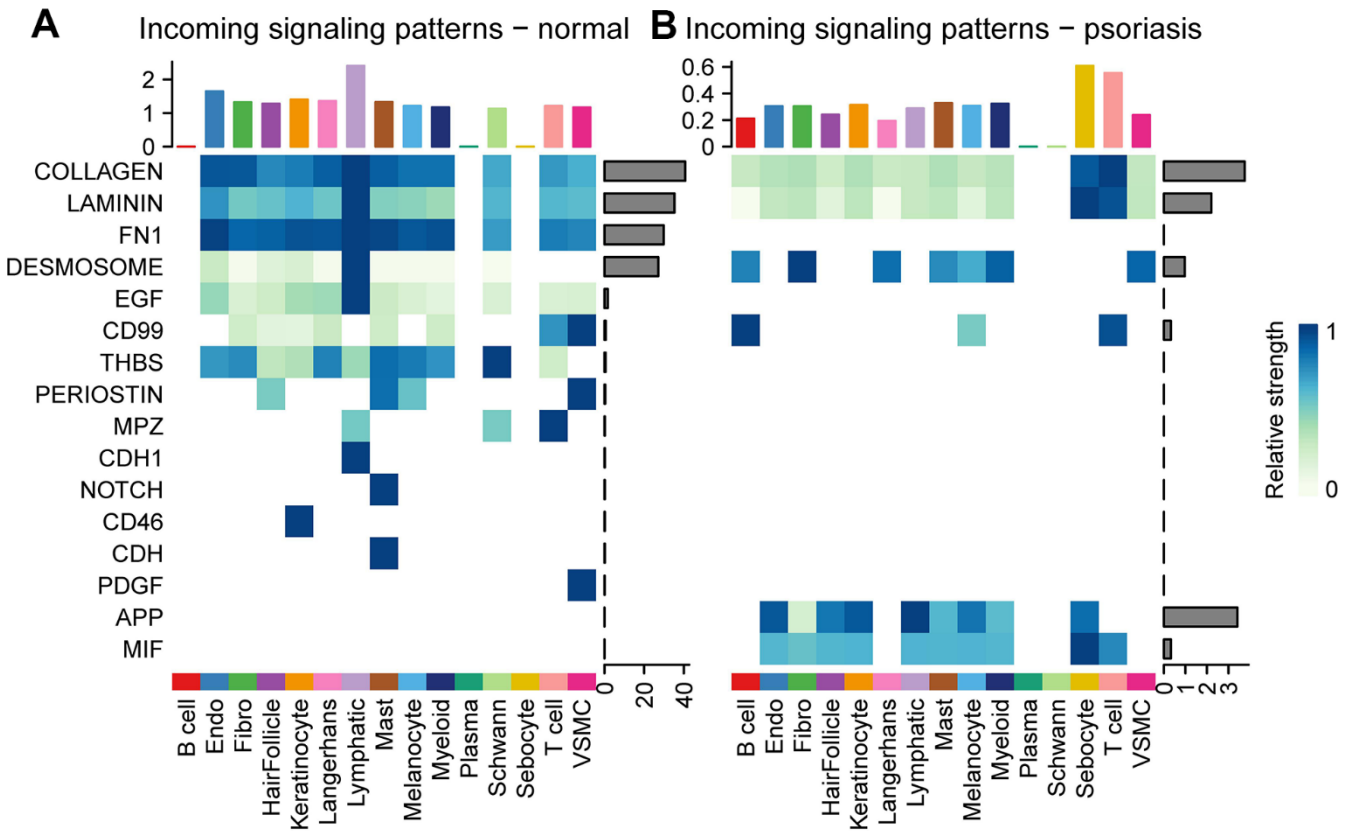

Supplementary Figure 2. Incoming signaling patterns for each subtype of cells in psoriatic and normal skin. (**A**) Normal skin. (**B**) Psoriasis.

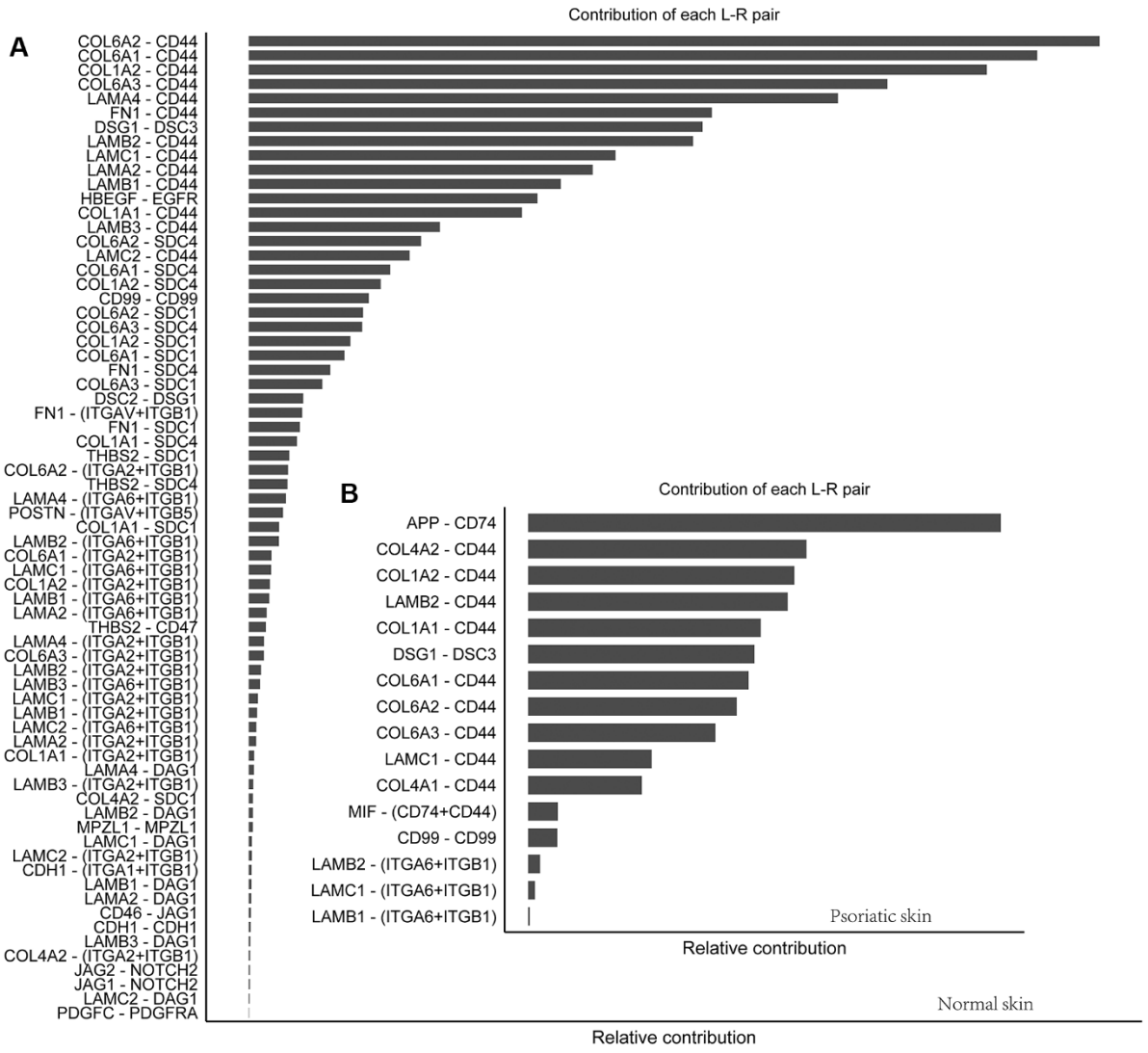

C

Detection status	Proportion	Ligand receptor
Detectable proteins in pathology sections	36 (36/80, 45%)	COL1A1, COL1A2, COL4A1, COL4A2, COL6A1, COL6A2, COL6A3, LAMA4, LAMA5, LAMB1, LAMB2, LAMC1, APP, DSC1, DSG1, NAMPT, MIF, ANGPTL2, THBS1, HSPG2, CD99, GRN, SELPLG, ITGA1, CD44, SDC1, ITGA6, DAG1, CD74, DSC3, NCL, CDH5, CD47, SORT1, ITGB1, ITGB4
Unidentified protein at the pathology section	44 (44/80, 55%)	MDK, TNFSF10, ANGPTL4, DLL1, DLL4, JAG2, VEGFB, PGF, APLN, SELE, TNF, MPZL1, ADM, EFNA1, EFNA5, SEMA6A, ICOSL, EFNB1, EFNB2, IGF2, SEMA7A, EDN1, TNFSF12, ITGA9, ITGA10, SDC4, INSR, ACKR3, TNFRSF10B, TLR4, NOTCH1, NOTCH4, VEGFR1, APLNR, TNFRSF1B, CALCRL, EPHA1, EPHA4, PLXNA2, ICOS, CTLA4, EDNRB, TNFRSF12A, CXCR2

Supplementary Figure 3. Contribution of ligand receptors (L-R) in normal skin and psoriatic skin. (**A**) Contribution of ligand-receptor pairs in normal skin. (**B**) Contribution of ligand-receptor pairs in psoriatic skin. (**C**) Expression of ligand receptor pairs in pathological tissue sections and the proportion of them detected. The data show that all ligand receptor pairs have been detected in psoriasis and that a relatively high proportion of ligand receptors in normal skin have also been detected for the most part.

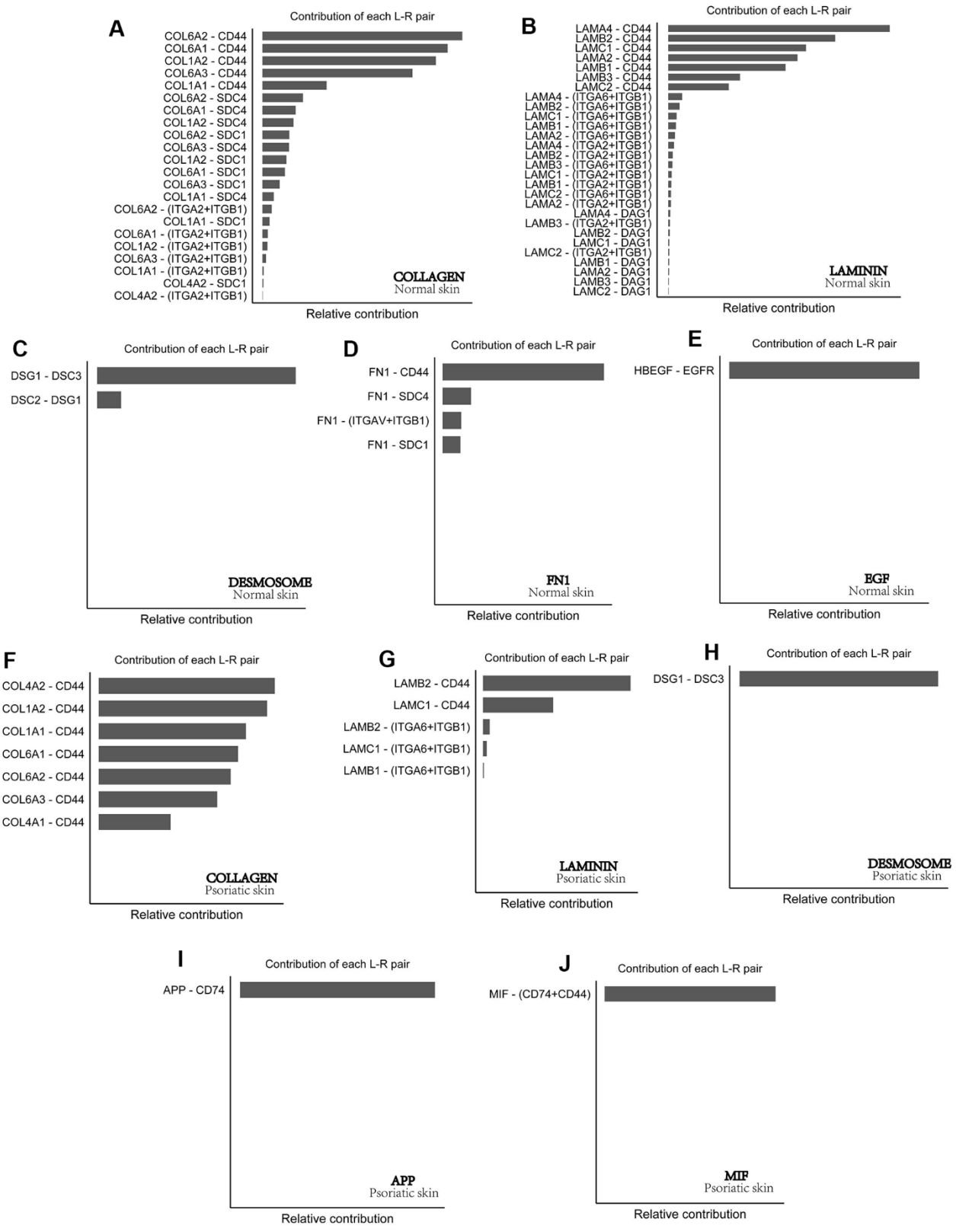

Supplementary Figure 4. Contribution of ligand receptor (L-R) in different signaling pathways in psoriasis and normal skin. (**A**–**E**) Contribution of ligand receptor pairs in five signaling pathways (COLLAGEN, LAMININ, FN1, DESMOSOME and EGF) in normal skin. (**F**–**J**) Contribution of ligand receptor pairs in five signaling pathways (COLLAGEN, LAMININ, DESMOSOME, APP and MIF) in psoriatic skin.

Supplementary Tables

Please browse Full Text version to see the data of Supplementary Tables 1, 3, 5, 7–9.

Supplementary Table 1. Demographic data for the psoriasis and normal samples used in the experimental validation section.

Supplementary Table 2. The cell type-specific regulons (CTSRs) in psoriasis.

Num.	Cell clusters	Number of regulons	Number of CTSRs	CTSRs
1	B cell	0	0	-
2	Endo	23	23	E2F7, ETS2, IRF3, TBX21, NFAC1, ZN467, SP2, VEZF1, SPIB, FLI1, KLF5, PRDM6, MAZ, ZN341, PTF1A, STAT1, PATZ1, ZN263, SP3, SP1, E2F6, WT1, CPEB1
3	Fibro	18	16	SP4, ZN350, LMX1A, TFE2, VEZF1, PATZ1, KLF12, ZN467, TBX1, ZN263, RXRA, CPEB1, SP1, ZN770, Z324A, SP3
4	Hair Follicle	5	2	VEZF1, ZNF770
5	Keratinocyte	32	32	SALL4, IRF3, ZN341, PBX1, TBX1, ZN467, COT1, NFIB, NFAC1, ZN263, SRBP2, EGR4, ETS2, TBX15, PRDM6, SPIB, RARB, KLF3, RXRA, WT1, FOXJ3, SP3, CPEB1, KLF1, PATZ1, MAZ, SP1, ZFX, SP2, ZN770, PITX2, VEZF1
6	Langerhans	0	0	-
7	Lymphatic	1	0	-
8	Mast	2	1	ZNF148
9	Melanocyte	0	0	-
10	Myeloid	3	0	-
11	Plasma	17	0	-
12	Schwann	16	0	-
13	Sebocyte	4	0	-
14	T cell	2	0	-
15	VSMC	7	2	CPEB1, SP2

Supplementary Table 3. Cellular subtype dataset for the distribution of cell type-specific regulons (CTSRs) and their target genes in psoriasis.

Supplementary Table 4. Human and mouse skin share overlapping cell type specific regulons (CTSRs).

Dataset	Overlapping regulons	All regulons	Method
Human skin in psoriasis	ETS2, IRF3, SP2, FLI1, KLF5, MAZ, STAT1, SP1, WT1, SP4, SALL4, SRBP2, FOXJ3, PITX2, ZN148, ZN281	ETS2, IRF3, SP2, FLI1, KLF5, MAZ, STAT1, SP1, WT1, SP4, SALL4, SRBP2, FOXJ3, PITX2, ZN148, ZN281, E2F7, TBX21, NFAC1, ZN467, VEZF1, SPIB, PRDM6, ZN341, PTF1A, PATZ1, ZN263, SP3, E2F6, CPEB1, ZN350, LMX1A, TFE2, KLF12, TBX1, RXRA, ZN770, Z324A, PBX1, COT1, NFIB, EGR4, TBX15, RARB, KLF3, KLF1, ZFX, KAISO, HXD13, RARA	IRIS3
Mouse skin cell (anagen, 5w)	ETS2, IRF3, SP2, FLI1, KLF5, MAZ, STAT1, SP1, WT1, SP4, SALL4, SRBP2, FOXJ3, PITX2, ZN281	ETS2, IRF3, SP2, SPIB, FLI1, KLF5, MAZ, STAT1, SP3, SP1, WT1, SP4, SALL4, SRBP2, KLF3, FOXJ3, ZFX, PITX2, ZN281, HMGA1, SPI1, STF1, ERR2, SALL1, ZN143, FUBP1, ETV2, NR5A2, BATF, EGR1, SRY, ELF5, FOXJ2, KLF15, ANDR, SP5, HNF6, BHA15, RXRG, SMAD4, RFX6, THA, KLF6, ZBT17, HAND1, FOXD3, STA5A, MYB, THA11, IRF4, ZN322, FOXQ1, RREB1, FOXD1, RUNX3, E2F1, MAFK	IRIS3
Mouse skin cell (telogen, 9w)	ETS2, IRF3, SP2, FLI1, KLF5, MAZ, STAT1, SP1, WT1, SP4, SALL4, SRBP2, FOXJ3, PITX2, ZN148, ZN281	ETS2, IRF3, SP2, FLI1, KLF5, MAZ, STAT1, SP1, WT1, SP4, SALL4, SRBP2, FOXJ3, PITX2, ZN148, ZN281, ESR1, RREB1, PRD16, OLIG2, STF1, GLI3, FUBP1, FOXJ2, SALL1, SP5, NR2C1, ELF5, PURA, EGR2, ANDR, ETV2, SOX9, SMAD3, ZBT17, SMAD2, KLF15, E2F3, IRF5, SMAD4, NFIC, RXRG, SRY, SPI1, ERR2	IRIS3

Supplementary Table 5. Proteins detected in pathological sections of psoriasis and normal skin and their protein profile.

Supplementary Table 6. Overlapping ligand receptors in protein assays in pathological sections of psoriasis and healthy skin.

Protein accession	Gene name
Q9UKU9	ANGPTL2
P05067	APP
P16070	CD44
Q08722	CD47
P04233	CD74
P14209	CD99
P33151	CDH5
P02452	COL1A1
P08123	COL1A2
P02462	COL4A1
P08572	COL4A2
P12109	COL6A1
P12110	COL6A2
P12111	COL6A3
Q14118	DAG1
Q08554	DSC1
Q14574	DSC3
Q02413	DSG1
P28799	GRN
P98160	HSPG2
P56199	ITGA1
P23229	ITGA6
P05556	ITGB1
P16144	ITGB4
Q16363	LAMA4
O15230	LAMA5
P07942	LAMB1
P55268	LAMB2
P11047	LAMC1
P14174	MIF
P43490	NAMPT
P19338	NCL
P18827	SDC1
Q14242	SELPLG
Q99523	SORT1
P07996	THBS1

Supplementary Table 7. Differential proteins in pathological sections of psoriasis and normal skin.

Supplementary Table 8. High overlap of differential proteins with target genes of cell type specific regulators (CTSRs) in psoriatic and healthy skin pathological areas.

Supplementary Table 9. Target genes of cell type specific regulons (CTSRs) overlap highly with proteins detected in psoriatic and healthy skin pathological areas.

Supplementary Table 10. Proportion of target genes for cell type specific regulators (CTSRs) detected in psoriasis and healthy skin pathology tissue sections.

Detection status	proportion	Target genes of cell type specific regulators (CTSRs)
Detectable proteins in pathology sections	674 (674/839, 80.3%)	TPM4, WDR1, RPL29, TPM1, TMSB4X, UBQLN1, YME1L1, PTBP3, RPL23, CCT3, PTPRF, PTBP1, RPS27A, SMARCC1, TPR, OSBPL8, RAB31, RPS12, SKP1, SUCLG1, PSMD1, RAC1, RPL8, RPL36, PSMD2, RPL12, RPL10A, RPL10, SH3BGRL3, YY1, UBE2K, TXN, PTMA, PUF60, RAB10, RSL1D1, RPL34, SEC62, USP15, NAA50, CYB5R3, PPIG, RPL27A, RPL28, VAMP8, RIOK3, RPL37A, RPL5, AHCY, SYNGR2, SPTBN1, VPS26A, VIM, PLS3, RPN2, HNRNPAB, SNRPD2, SFPQ, SLPI, RPL32, SERF2, RPS14, S100A14, SUB1, TCP1, TGOLN2, CCT2, STAT1, RANGAP1, RAD23B, PRNP, SBSN, SOD2, SET, TXNDC17, TYMP, PSMB7, RPL26, RPL4, ROCK2, UTRN, VWF, XRCC6, RPL6, TPM3, ATP6V1F, ATP6V1G1, OS9, PSMA6, RPL30, RPLP2, UQCR10, SON, RAB34, REEP5, RHOA, RHOC, RPL14, RPL13A, RPL39, POLR2L, POLR1D, MRPL12, SSR4, CCT8, XRCC5, RRBP1, RPS19, RPS16, RPS28, SRP72, SRP14, TERF2IP, NDUFS5, TM9SF3, PSMD7, RPL24, RPL31, TPSAB1, RPLP0, TRIM29, RPS13, RPS15A, YBX3, RPS21, S100A16, CCT5, TUBB2A, UBXN1, ZFP36, ZC3H15, UBXN4, TIMM13, TUBB4B, TXNIP, ZNF207, ZNF385A, VDAC1, RPS3, SLK, TIMP1, THY1, USP47, WNK1, PCOLCE, PLVAP, PSMB5, RPL36AL, SPARC, ZBTB20, HDLBP, RBM25, UBL5, WAC, ZFP91, YWHAB, YWHAQ, ACTG1, CBR1, CCDC80, CD93, ANGPTL2, COL5A1, COL6A3, BTF3, BAG1, BICD2, CYB5A, DCTN3, CAV1, CAPZB, DEK, DDX21, DDX3X, CFH, CD63, COX5A, EGFR, NT5E, HSPE1, AP2S1, ATP1A1, ANXA2, CTSG, PSIP1, CLTA, HSPA5, CALR, DAB2, CDH11, CHD4, COX7C, DPYSL3, EIF1, EEF2, IFI16, CAPRIN1, CKAP4, CNBP, COL1A2, EDF1, CTNNB1, G3BP1, DSTN, HADHA, ECHS1, GSN, BAIAP2, SLC25A5, CAPG, CPD, CPA3, ARPC5, COL1A1, CSDE1, TMBIM6, BRK1, CYBRD1, CALD1, CALU, COL4A1, GSPT1, FUS, FTL, DBI, GOT2, AKAP13, PYCARD, CRTAP, COPS6, COX5B, COX6C, BCAP31, BAG3, CAP1, C1S, COX7A2, A2M, ABLIM1, YWHAZ, CTSK, CD44, CLUH, CFL1, CSTA, GRN, HMGCS1, HMGA1, AHNAK, APRT, ACTR3, ARPC2, EPB41L2, DSC2, EBNA1BP2, DSC3, DYNC1H1, EIF3M, GPNMB, EEA1, CSTB, GGCT, ARHGDIA, ENO1, EIF3D, GUK1, PKM, HSPA9, ALDOA, CAPN1, ARL8B, ANP32B, ACTR2, ARPC5L, CNN3, COL18A1, CCAR1, DDX1, CST3, SFN, DEGS1, SDF4, CD99, EI24, CTNNA1, COX6B1, GBP2, FAM162A, ENSA, GSTP1, YWHAG, APP, ALDH2, ALDH3A2, AKR1B10, AQP3, ANXA1, ATP2A2, CCDC50, CHMP2A, CD9, COX4I1, CYCS, GNG12, GNG11, ITGA6, AEBP1, ANXA5, SYNCRIP, EIF5, EIF6, LRP1, MAN1A1, METAP1, MBD2, LAMC1, LAMP2, KTN1, MDH2, MAL2, NCL, MYL12B, CD59, CD81, CLTB, COL3A1, COL5A2, CLIC4, COL6A1, COL6A2, FBLN2, GLG1, HSPH1, HSPA4L, HNRNPF, PPA1, IQGAP1, IMPDH2, LYPD3, MTDH, LUM, MAPK13, CDC42, EZR, ILF2, EIF4A3, EIF5B, EIF4B, SERPING1, CD74, MAP7D1, LY6D, MGLL, MFAP4, FDPS, GHITM, EIF2S1, GNG5, HSP90AB1, HNRNPC, HNRNPU, LRRFIP1, IDH2, IDI1, MBNL1, EIF4A1, IGFBP7, LAMB1, KRTDAP, CLU, DSG1, DSG3, CLCA2, DDX17, EIF3B, EEF1A1, FGFBP1, PERP, NDUFB9, NDUFB10, NHP2, CALM1, CEBPD, CIRBP, DYNLL1, COL15A1, CYC1, CTR9, FLNA, ETF1, ESRP1, FSTL1, HSD17B10, HTRA1, MSN, DRAP1, NDUFB4, SLC25A6, GJA1, CDH1, DDX5, DSP, DIAPH1, ENAH, TUFM, FMOD, FBN1, FBLN1, LAMA4, RPS6KB2, FTH1, LGALS3, LPAR1, NFIX, NNMT, NUCKS1, NAA15, CALML3, CTSD, DNAJA1, EIF3J, EIF3I, ITM2B, PDAP1, CCDC47, ATP1B3, HSPD1, DHCR24, EIF3H, GLUL, GNA15, GNAI2, GLTP, SLC2A1, HEBP2, HNRNPD, KHDRBS1, HSPA8, IFITM3, EIF2S2, NFKBIA, HK1, MMP2, AK2, LAD1, NSA2, NPM1, OLFML3, OPTN, ENG, EIF3E, EIF3L, VCAN, DAD1, DNAJB1, EIF3A, HSP90B1, ITGA5, KRT1, SERBP1, PDLIM1, IGFBP4, MCL1, MATR3, EIF4G2, MARCKS, MX1, JUP, PPP1CA, PPP1CB, PSMA4, GPX4, LAMP1,

		HSP90AA1, KPNB1, JUNB, JUND, ITGB5, PARK7, PALLD, PLP2, HINT1, NDUFS7, NME1, NDRG1, NOLC1, NDUFA4, NDUFA10, MYL6, IMPA2, LGALS3BP, SLC16A10, PRDX1, PRDX5, NRP1, RBM3, P4HB, PDIA3, PDIA6, PSMC5, PSMB1, HSPA4, NACA, PA2G4, PGRMC1, PDGFRB, PEA15, UQCRQ, C6orf132, CHCHD2, CD82, GAPDH, HDGF, HNRNPDL, IL6ST, ITGB1, PSMC2, CSNK1A1, LGALS1, HNRNPK, PAFAH1B1, KLF5, MXRA5, NDUFV1, PSMB6, RBM39, GOLGA4, NDUFA13, PAPOLA, DCN, SFRP2, SLIT3, SNRPD3, TOLLIP, SRSF11, DNTTIP2, GLO1, MACF1, PFDN5, PABPC1, PRPF40A, RAD21, RAB1A, RAB25, RPL27, RPL38, S100A4, S100A6, S100A7, S100A8, S100A9, S100A10, S100A11, SAP18, SEC61B, PTP4A2, FAM114A1, RPL22, RPL23A, RPS23, RPS24, SNRPB, MRPS34, PKP3, PSMA3, PPIB, UQCRH, CRABP2, MRPL27, RPL13, PSMD8, HNRNPA2B1, RPS6, PTGES3, SNX9, SRGN, TPI1, RPL19, SF3B1, RPS15, CCT6A, TAF7, PCBP2, PKP1, SEC31A, TUBA4A, SRSF3, STK24, U2SURP, RPS5, TALDO1, TAGLN2, GM2A, SDC1, AHCYL1, NAPA, TMEM45A, TIMM8B, SPINT2, STAT3, SWAP70, GNB1, GDI2, CAST, EIF4G1, PSMA7, RAB3D, RPS29, HSPB1, MYH9, NCKAP1, HSPG2, PRRC2C, HNRNPM, NDUFS6, METAP2, MAP4, UQCRB, RAB7A, RPL18, RPLP1, RPL3, RRAGC, SOD1, SH3GLB1, RPS20, RPS11, SERPINB4, TMEM245, TMED3, PCBP1, PPL, PHB2, RPL11, PSMC3, RPL15, TUBA1C, SRSF2, TMED9, MZT2B, RPS8, RPS2, RPSA, TACC1, TACSTD2, VCP, SERPINB5, SPCS1, MSMO1, PEBP1, PGK1, NOP58, RPL35, NDUFB7, PMVK, PPP3CA, PLEKHO2, PLIN3, PLXND1, ARHGAP18, PRRX1, RPS7, FAU, RTN4, SYNE2, LTBP1, MPZL2, SLC25A3, RAN, PFN1, PSMB4, PPIA, RPL35A, STOM
Undetectable proteins at the pathology sections	165 (165/839, 19.7%)	EPAS1, TCF4, TGFBR2, TM4SF1, EMP1, NUAK1, EMCN, ETS2, SPARCL1, ATP8B1, EVA1C, HIPK3, OLFM1, CAV2, PIK3C2A, SNRK, TSC22D1, TNFRSF10D, ETS1, RALGAPA2, ATF4, CDKN1A, FOXP1, ITM2A, PRKCH, PTTG1IP, BMPR2, ECE1, FLT1, PRSS23, WWTR1, CCNI, IFITM2, JAK1, SH3BP5, ADAMTSL4-AS1, DUSP6, APLP2, ARID5B, ATF3, EID1, FOS, GADD45B, IER5, RHOB, RPL37, ZFP36L1, ZFP36L2, CRISPLD2, APCDD1, TIMP2, F2R, LAPTM4A, ACTB, FGFR1, IL1R1, PMP22, TMEM176B, DDR2, PAM, NUPR1, PLAC9, SERINC1, ANTXR1, ID2, REV3L, NR4A1, ARRDC3, AKAP9, ARF1, DMKN, FXYD3, SNHG5, TSPO, ZFAS1, C4orf3, KRT10, KRT6A, SCD, EMP2, SPTSSA, MAFB, CA12, KRT16, NRARP, NSG1, COX8A, DUSP1, EGR1, IER2, OST4, SLC39A6, TMEM123, RHOV, CALM2, GADD45GIP1, MAF, RALBP1, UBE2D3, EHF, GJB2, BHLHE40, COX6A1, COX7B, EFNA1, MAPK6, MRFAP1, RND3, SNHG8, CAMLG, NFE2L2, PTP4A1, RAB11A, TOMM20, C19orf33, C1orf21, KLF4, NDUFB2, PYURF, SERP1, BPTF, NFE2L1, ALDH3B2, C11orf58, C1orf43, MRPL51, NDUFA1, POMP, PPP2CA, ROMO1, SLC25A39, TOMM7, MYL12A, RORA, MXD1, SPPL3, ANKRD12, AURKAIP1, FOSB, GAS5, PNRC1, PPDPF, RNF11, RSRC2, SLC38A2, TMEM154, TNFAIP3, ZC3H12A, ZDHHC3, SCAF11, SCO2, BMP2K, KIT, LAPTM5, BTG1, MALAT1, OAZ1, JUN, PPP1R15A, UBA52, UBB, UBC, KLF6, SLU7, NFKBIZ

Supplementary Table 11. KEGG pathway enrichment analysis of Q1 protein in psoriasis pathology tissue sections.

KEGG pathway	Mapping	Background	All mapping	All background	Fold enrichment	Fisher's exact test p-value	-log10 (p-value)	Related proteins
hsa04610 Complement and coagulation cascades	21	64	149	2834	6.24	2.02707152308558E-12	11.69	P00747 P04004 P13671 P01024 P08697 P00742 P04003 P0C0L5 P02679 P03952 P10909 P02748 P07357 P02675 P08174 P02671 P00748 P05154 P05546 P01042 P00734
hsa05143 African trypanosomiasis	5	14	149	2834	6.79	0.000511397243201717	3.29	P69905 P02647 P50148 P68871 P01042
hsa03320 PPAR signaling pathway	7	38	149	2834	3.5	0.00306959200311731	2.51	Q9BX66 Q99541 P23786 P02647 P02652 O15540 O60240
hsa00860 Porphyrin metabolism	4	15	149	2834	5.07	0.00635633605691733	2.2	P00450 P13716 P30519 P30043
hsa04080 Neuroactive ligand-receptor interaction	4	16	149	2834	4.76	0.00813377948573137	2.09	P00747 P01024 P01042 P00734
hsa00340 Histidine metabolism	3	13	149	2834	4.39	0.0276072194693599	1.56	P43353 P21397 P30837
hsa00910 Nitrogen metabolism	2	6	149	2834	6.34	0.0358187358419433	1.45	P00915 P00918
hsa04371 Apelin signaling pathway	7	61	149	2834	2.18	0.0387258116740504	1.41	P10301 Q15796 P62879 P61952 Q14344 P50148 O60240
hsa05310 Asthma	3	15	149	2834	3.8	0.0406756033570966	1.39	P13727 P11678 P30273
hsa05150 Staphylococcus aureus infection	6	50	149	2834	2.28	0.0448414576181837	1.35	P00747 P01024 P0C0L5 P12314 P02679 Q92764
hsa04978 Mineral absorption	3	16	149	2834	3.57	0.0481852550196982	1.32	P02787 Q53TN4 P30519

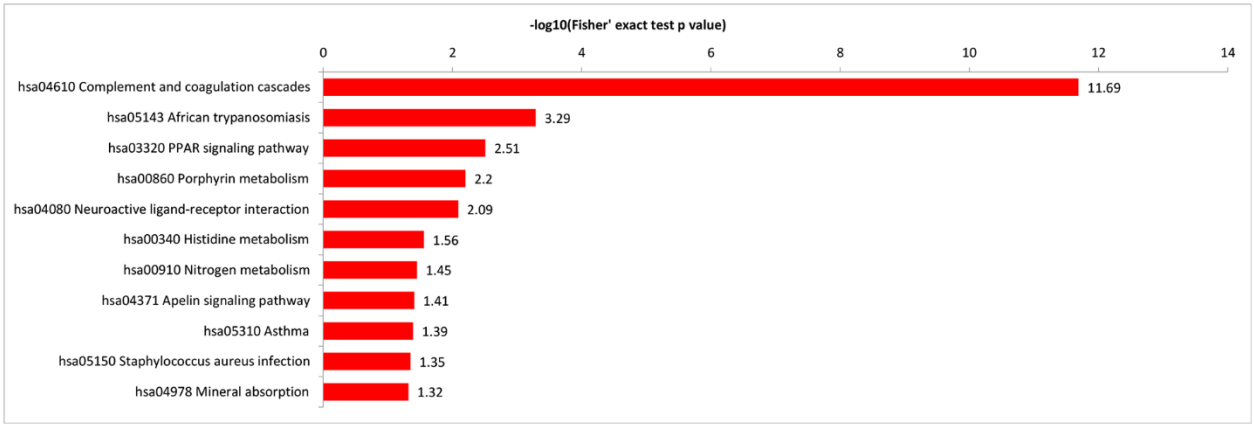
-log10(Fisher' exact test p value)
0
2
4
6
8
10
12
14
hsa04610 Complement and coagulation cascades
11.69
hsa05143 African trypanosomiasis
3.29
hsa03320 PPAR signaling pathway
2.51
hsa00860 Porphyrin metabolism
2.2
hsa04080 Neuroactive ligand-receptor interaction
2.09
hsa00340 Histidine metabolism
1.56
hsa00910 Nitrogen metabolism
1.45
hsa04371 Apelin signaling pathway
1.41
hsa05310 Asthma
1.39
hsa05150 Staphylococcus aureus infection
1.35
hsa04978 Mineral absorption
1.32

Supplementary Table 12. KEGG pathway enrichment analysis of Q2 protein in psoriasis pathology tissue sections.

KEGG pathway	Mapping	Background	All mapping	All background	Fold enrichment	Fisher's exact test p-value	-log10 (p-value)	Related proteins
hsa04510 Focal adhesion	9	108	73	2834	3.24	0.00152731665240096	2.82	O75116 P49746 Q03135 Q05397 O75369 Q14315 P46108 Q13418 P27361
hsa04012 ErbB signaling pathway	5	41	73	2834	4.73	0.00359370028970315	2.44	P42229 Q05397 P46108 P27361 Q13557
hsa05150 Staphylococcus aureus infection	5	50	73	2834	3.88	0.0084905104569172	2.07	P09871 P02747 P28067 P05156 P19012
hsa05322 Systemic lupus erythematosus	5	52	73	2834	3.73	0.0100084069452076	2	P09871 P02747 P28067 Q16778 P19474
hsa04658 Th1 and Th2 cell differentiation	4	36	73	2834	4.31	0.0128006221416951	1.89	P42229 P28067 P27361 P42226
hsa05220 Chronic myeloid leukemia	4	38	73	2834	4.09	0.0154332453003611	1.81	P42229 Q92466 P46108 P27361
hsa03320 PPAR signaling pathway	4	38	73	2834	4.09	0.0154332453003611	1.81	P33121 P02656 Q13418 Q96Q06
hsa04360 Axon guidance	5	58	73	2834	3.35	0.0156627070676531	1.81	O75116 Q05397 Q13418 P27361 Q13557
hsa05205 Proteoglycans in cancer	7	105	73	2834	2.59	0.0170927890779721	1.77	O75116 Q03135 Q05397 O75369 Q14315 P27361 Q13557
hsa04610 Complement and coagulation cascades	5	64	73	2834	3.03	0.0231418008993157	1.64	P09871 P02747 P01008 P05155 P05156
hsa05133 Pertussis	4	43	73	2834	3.61	0.023434380351256	1.63	P09871 P02747 P05155 P27361
hsa05213 Endometrial cancer	3	25	73	2834	4.66	0.0251186449158574	1.6	Q92466 Q13418 P27361
hsa04659 Th17 cell differentiation	4	44	73	2834	3.53	0.0252873210209065	1.6	P42229 P28067 P27361 P42226
hsa05161 Hepatitis B	5	66	73	2834	2.94	0.0260736942665817	1.58	P42229 Q92466 Q7Z434 P27361 P42226
hsa04935 Growth hormone synthesis, secretion and action	4	48	73	2834	3.24	0.0335697440257818	1.47	P42229 Q05397 P46108 P27361
hsa00790 Folate biosynthesis	2	12	73	2834	6.47	0.0365577557963611	1.44	P35270 Q9NQX3
hsa04261 Adrenergic signaling in cardiomyocytes	4	50	73	2834	3.11	0.0382408441834425	1.42	P09493 Q93084 P27361 Q13557
hsa04062 Chemokine signaling pathway	5	74	73	2834	2.62	0.0401396137908071	1.4	O75116 Q05397 P46108 P27361 Q8TCU6
hsa04217 Necroptosis	5	75	73	2834	2.59	0.0421690998597402	1.38	P42229 Q96EP0 P06737 Q13557 P42226

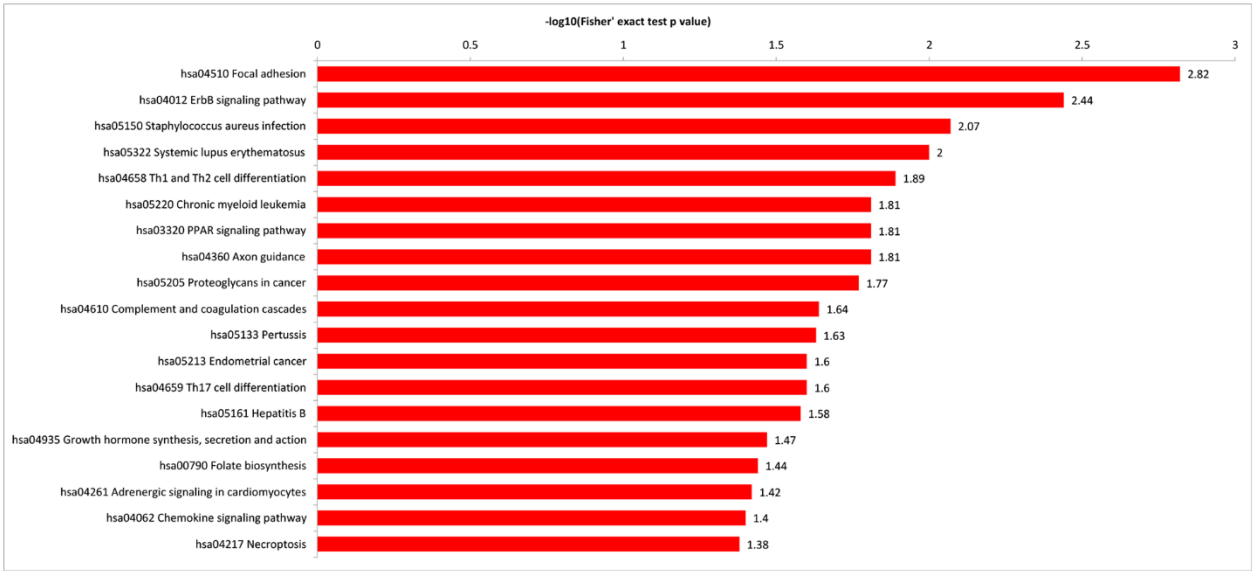
-log10(Fisher' exact test p value)
0
0.5
1
1.5
2
2.5
3
hsa04510 Focal adhesion
2.82
hsa04012 ErbB signaling pathway
2.44
hsa05150 Staphylococcus aureus infection
2.07
hsa05322 Systemic lupus erythematosus
2
hsa04658 Th1 and Th2 cell differentiation
1.89
hsa05220 Chronic myeloid leukemia
1.81
hsa03320 PPAR signaling pathway
1.81
hsa04360 Axon guidance
1.81
hsa05205 Proteoglycans in cancer
1.77
hsa04610 Complement and coagulation cascades
1.64
hsa05133 Pertussis
1.63
hsa05213 Endometrial cancer
1.6
hsa04659 Th17 cell differentiation
1.6
hsa05161 Hepatitis B
1.58
hsa04935 Growth hormone synthesis, secretion and action
1.47
hsa00790 Folate biosynthesis
1.44
hsa04261 Adrenergic signaling in cardiomyocytes
1.42
hsa04062 Chemokine signaling pathway
1.4
hsa04217 Necroptosis
1.38

Supplementary Table 13. KEGG pathway enrichment analysis of Q3 protein in psoriasis pathology tissue sections.

KEGG pathway	Mapping	Background	All mapping	All background	Fold enrichment	Fisher's exact test p-value	-log10 (p-value)	Related proteins
hsa03010 Ribosome	31	106	172	2834	4.82	1.59332166405189E-14	13.8	P62829 P30050 P62906 P46776 P08708 P62701 P82932 P62424 P22090 Q02878 P62888 P05387 P62249 P62857 P83731 P18124 P05388 P62277 P62244 P61353 P63173 P62750 P62847 P84098 P46782 P62851 Q07020 P60866 P62913 P61313 P18077
hsa05171 Coronavirus disease - COVID-19	33	155	172	2834	3.51	3.80877076730991E-11	10.42	P62829 P30050 P62906 Q99836 P46776 P08708 P62701 P62424 P22090 Q02878 P62888 P05387 P62249 P62857 P83731 P18124 P05388 P62277 P62244 O95786 P61353 P63173 P62750 P62847 P84098 P46782 P62851 P40763 Q07020 P60866 P62913 P61313 P18077
hsa03015 mRNA surveillance pathway	9	58	172	2834	2.56	0.00729283044126032	2.14	Q13310 Q9UKF6 P35637 O43809 P62495 Q86U42 P62136 P51003 Q86V81
hsa00760 Nicotinate and nicotinamide metabolism	4	16	172	2834	4.12	0.0134076491169586	1.87	P00491 P49902 Q06278 P43490
hsa00970 Aminoacyl-tRNA biosynthesis	5	27	172	2834	3.05	0.0210625411587651	1.68	Q9Y285 Q15046 P12081 P26639 P49591
hsa03040 Spliceosome	13	117	172	2834	1.83	0.0279485728569399	1.55	Q9BWJ5 O14776 Q9Y2W2 Q86XP3 P35637 P55769 O60828 Q86V81 P62304 P09651 O15042 Q96FV9 Q9Y3C6
hsa00750 Vitamin B6 metabolism	2	5	172	2834	6.59	0.0324291844550689	1.49	Q9Y617 Q06278
hsa03050 Proteasome	6	41	172	2834	2.41	0.0349861796654851	1.46	Q9UL46 P51665 Q06323 P62195 O14818 O00487
hsa03008 Ribosome biogenesis in eukaryotes	7	52	172	2834	2.22	0.0354229688789109	1.45	Q8NI36 Q9Y3A5 Q8IWA0 Q8N5L8 Q9H0D6 P55769 P62826
hsa00240 Pyrimidine metabolism	5	33	172	2834	2.5	0.0462387361397857	1.33	P00491 P19971 P49902 Q9H773 P15531
hsa04623 Cytosolic DNA-sensing pathway	4	23	172	2834	2.87	0.0468842339601234	1.33	P62875 O95786 Q9ULZ3 Q14116

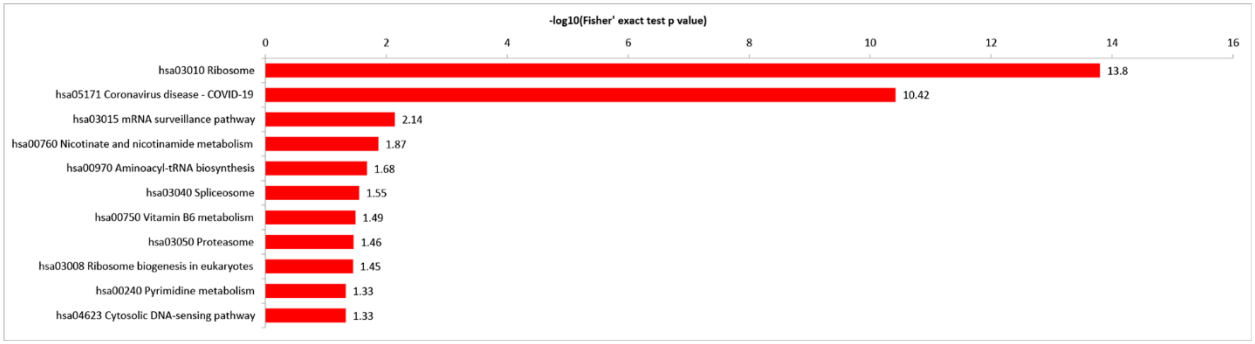
-log10(Fisher' exact test p value)
0
2
4
6
8
10
12
14
16
hsa03010 Ribosome
13.8
hsa05171 Coronavirus disease - COVID-19
10.42
hsa03015 mRNA surveillance pathway
2.14
hsa00760 Nicotinate and nicotinamide metabolism
1.87
hsa00970 Aminoacyl-tRNA biosynthesis
1.68
hsa03040 Spliceosome
1.55
hsa00750 Vitamin B6 metabolism
1.49
hsa03050 Proteasome
1.46
hsa03008 Ribosome biogenesis in eukaryotes
1.45
hsa00240 Pyrimidine metabolism
1.33
hsa04623 Cytosolic DNA-sensing pathway
1.33

Supplementary Table 14. KEGG pathway enrichment analysis of Q4 protein in psoriasis pathology tissue sections.

KEGG pathway	Mapping	Background	All mapping	All background	Fold enrichment	Fisher's exact test p-value	-log10 (p-value)	Related proteins
hsa03008 Ribosome biogenesis in eukaryotes	11	52	101	2834	5.94	1.21977150331164E-06	5.91	Q9UBU9 Q969X6 Q15061 Q8TED0 O60832 Q9BVP2 Q9BZE4 Q96G21 Q9ULX3 Q9H583 Q99575
hsa03010 Ribosome	11	106	101	2834	2.91	0.00112242705906763	2.95	Q9Y3D3 P40429 P52815 P39019 P18621 P63220 Q6P5R6 P62273 P39023 P15880 P62081
hsa05171 Coronavirus disease - COVID-19	13	155	101	2834	2.35	0.00289190376123779	2.54	Q9Y6K5 P40429 P39019 P18621 P63220 O14920 P20591 Q6P5R6 P62273 P39023 P15880 P19174 P62081
hsa04657 IL-17 signaling pathway	5	33	101	2834	4.25	0.00558227404580776	2.25	Q86SG5 O14920 P31151 P05109 P06702
hsa00790 Folate biosynthesis	3	12	101	2834	7.01	0.00764639209240929	2.12	P09417 O60218 Q92820
hsa05418 Fluid shear stress and atherosclerosis	7	67	101	2834	2.93	0.00890393646028822	2.05	O14920 O15217 Q9NZT1 P16284 P27482 P35052 Q14145
hsa01523 Antifolate resistance	3	13	101	2834	6.48	0.00968582937230774	2.01	O14920 Q92820 P33527
hsa04744 Phototransduction	2	5	101	2834	11.22	0.0117229388047486	1.93	Q9NZT1 P27482
hsa04070 Phosphatidylinositol signaling system	5	40	101	2834	3.51	0.012711195462184	1.9	Q9NZT1 P27482 O14732 Q13613 P19174
hsa04060 Cytokine-cytokine receptor interaction	3	15	101	2834	5.61	0.0146322830649248	1.83	Q9UBH0 P18510 Q9NZH8